

Under Distribution Limitation
Until February 28, 1987

NASA
LARGE-SCALE ADVANCED
PROP-FAN
(LAP)
HUB/BLADE RETENTION
DESIGN REPORT

By: Matthew Soule

HAMILTON STANDARD DIVISION
UNITED TECHNOLOGIES CORPORATION

Prepared For
National Aeronautics and Space Administration
NASA-Lewis Research Center
Contract NAS3-23051

January 31, 1986



CONTENTS

<u>SUBJECT</u>	<u>PAGE</u>
SUMMARY	1
INTRODUCTION	3
RETENTION AND HUB LOADS	5
TAILSHAFT LOADS	13
BLADE RETENTION STRESS	15
BARREL STRESS	21
TAILSHAFT	27
SPRING RATE	31
WEIGHTS	41
CONCLUSION	43
REFERENCES	45
APPENDIX A	47
APPENDIX B	69

PRECEDING PAGE BLANK NOT FILMED

FIGURES

<u>Figure</u>		<u>Page</u>
1	Hub and Blade Retention	6
2	Angle of Attack - Alpha	7
3	Loading - Aerodynamic-Cyclic	8
4	Blade Loading Coordinate System	10
5	Hub Loading	12
6	Retention	16
7	Blade Bearing Stress Criteria	17
8	Race Hardening	18
9	Subsurface Race Stress	19
10	Race and Ball Stress Criteria Subsurface Octahedral Shear Stress	20
11	Hub - Load Resolution	22
12	Ring Section Properties	23
13	Ring Section Properties	24
14	Blade, Race, Hub Arm Model	25
15	Ring and Arm Stress Criteria Machined Surfaces	26
16	Tailshaft Model	28
17	Tailshaft Stress Criteria	29
18	Propeller Frequencies Vs. Total Hub Spring Rate	32
19	Hub Segment	33
20	Bridge Section Properties	34
21	Bridge Section Properties	35
22	Hub Arm Bridge Section Properties	36

PRECEDING PAGE BLANK NOT FILMED

FIGURES (Continued)

<u>Figure</u>		<u>Page</u>
23	Bearing O.D. Vs. Spring Rate	38
24	Hub Spring Rate in *Lb/Rad* 10°	39
25	Hub and Retention Weight	42



SUMMARY

The Large Scale Advanced Prop-Fan hub assembly forms a semi-rigid link between the blades, which provide the thrust, and the engine shaft, which provides the torque. The hub and tailshaft is a one piece partially forged part which is carburized, heat treated and machined. A single row ball bearing restrains each of the eight blades in the hub, while the tailshaft secures the propeller to the engine shaft with two cone seats that are preloaded against each other by the Prop-Fan retaining nut. The hub also forms the support for the pitch change actuator system, the control and the spinner.

The retention transmits the loads from the blades to the hub while allowing the changes in blade pitch. The single row ball bearing retention provides ease of maintenance by allowing individual blade replacement without disassembly of the hub. It has a through hardened inner race which seats against the aluminum blade shank and an outer race which is integral with the barrel. The outer race area is carburized to achieve the hardness necessary to support the ball loads. The balls are kept from contact with each other by a separator. The rotational speed of the propeller keeps the retention submerged in the oil which is contained in the hub by a seal.

The hub assembly, because it is the foundation of the blade, also is an integral part of the mechanism which determines the natural frequencies of the propeller system. Analysis assured that none of these modes intersect with the operating frequencies of the Prop-Fan.

The hub portion of the assembly was designed to the same requirements which would be established for a production Prop-Fan (lightweight). Because the LAP is destined for test on an existing gearbox, and must accommodate an existing propeller control, the tailshaft portion of the assembly is identical to the 54H60 propeller tailshaft. Production Prop-Fans could incorporate either a tailshaft or a flange dependent on the reduction gearbox configuration.



INTRODUCTION

In recent years, considerable attention has been directed toward improving aircraft fuel consumption. Studies have shown that the inherent efficiency advantage that turboprop propulsion systems have demonstrated at lower cruise speeds may not be extended to the higher speed of today's turbofan and turbojet-powered aircraft. To achieve this goal, new propeller designs which feature more blades with thin airfoils and aerodynamic sweep are required.

Since 1975, Hamilton Standard has been deeply involved with the NASA Lewis Research Center in the development of the advanced turboprop or Prop-Fan. Many aircraft system studies have been accomplished for a variety of subsonic air transport applications and all these studies have shown significant fuel savings with Prop-Fan propulsion. The fuel savings potential of future Prop-Fan powered aircraft is generally 15-20% for commercial applications and 25-35% for military patrol aircraft compared to equal technology turbofan systems, depending upon the specific application, cruise speed, stage length and other requirements.

To date, several models have been designed, manufactured and subjected to a number of tests. A series of small-scale 0.6223 meter (24.5 inch) diameter module tests have been conducted in both UTRC and NASA wind tunnels and on a modified NASA airplane. These tests have shown that propellers with 8-10 swept blades, high tip speeds and high power loadings can offer increased fuel efficiencies at speeds up to 0.8 Mn.

HSD has designed a 2.743 meter (9-foot) diameter single-rotation Prop-Fan. Following the manufacture of the Prop-Fan system, it will be tested at Wright Field and in the ONERA S-1 wind tunnel in France. The hardware will then be used in a follow-on program where it will be run with an engine on a static test stand and on a research aircraft. The major objective of this testing is to establish the structural integrity of large-scale Prop-Fans of advanced construction in addition to the evaluation of aerodynamic performance and aero-acoustic design.

The report which follows covers the design analysis of the Large-Scale Advanced Prop-Fan Hub/blade retention assembly. Specifically, analysis of the retention area of the blade shank, blade retention, hub, and tailshaft are covered. Subjects included are stress and strain analysis, material hardness requirements, weight predictions and stiffness characteristics.

PRECEDING PAGE BLANK NOT FILMED

RETENTION AND HUB LOADS

A cross section through the hub and retention is shown in Figure 1. All the external loads on the retention and hub have their source in the blade loads. An understanding of the hub loads requires an explanation of those blade loads that are transferred to the hub. The loads on the blade are derived from the aerodynamic and inertia characteristics of the blade.

The aerodynamic loads generated by the moving airfoil blade sections are the lift and drag shear forces. On a particular blade (fixed geometry) these forces vary with changes in propeller rpm, aircraft speed, induced velocity vector and the blade angle. How these parameters affect the forces is determined as follows: the aircraft direction of flight and propeller rotation are vectorially combined to single velocity vector R , and the angle of attack ALPHA is the difference between the angular position of R and the blade angle. See Figure 2. The product of ALPHA times the slope of curves of lift and drag coefficients vs ALPHA is lift and drag coefficients. An examination of the lift and drag force equations show that these forces vary as the square of the velocity resultant R and directly with the lift and drag coefficients.

These aerodynamic loads are actually pressure distributions around the face and camber sides of the airfoil and along the axis of the blade but they may be depicted as concentrated forces, the lift and drag, acting at centers of pressure on the airfoil cross sections and along the blade axis. The center of pressure on the airfoil cross section is approximately one quarter chord from the leading edge. The offset of this point from the pitch change axis of the blade retention causes aerodynamic twisting moments, ATM, about the blade axis.

The center of pressure along the blade axis is in the tip region of the blade and the composite lift and drag forces there produce shear forces and moments that are reacted at the blade retention on the hub. The effect of the shear forces on the hub is minute compared to the moment effects.

If the aerodynamic loads on the blade are constant as the blade rotates, then the loads they produce at the blade retention on the hub are the steady bending moment and steady ATM.

When the aircraft climbs the aerodynamic loads on the blade become cyclic. The airflow into the propeller is no longer perpendicular to the plane of rotation. As the blade rotates its attitude relative to the fixed angular inflow changes, that is, its leading edge at one point would be up relative to the flow while at 180 degrees from that point it is down. This causes changes in the resultant velocity vector R as well as the angle of attack as the blade rotates. This change is sinusoidal on each blade and the retention sees this as a vibratory shear and bending moment. The blade moment loads add at the centerline of the Prop-Fan and produce a steady moment vector and shear force through which the tailshaft rotates. See Figure 3.

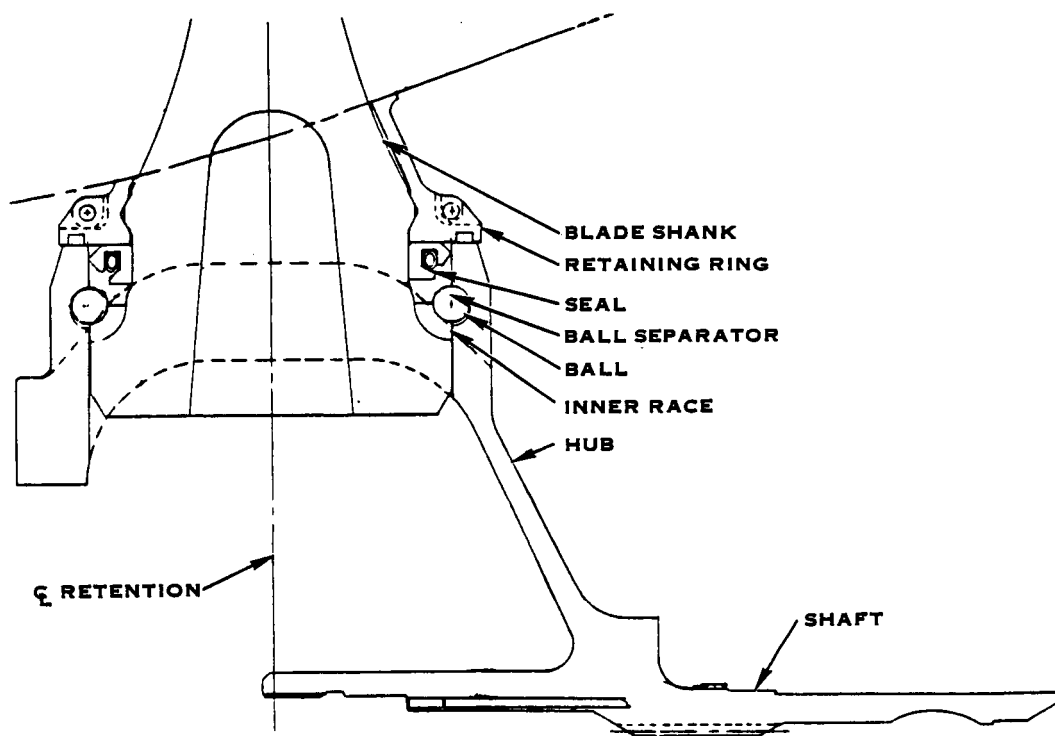


FIGURE 1. HUB AND BLADE RETENTION

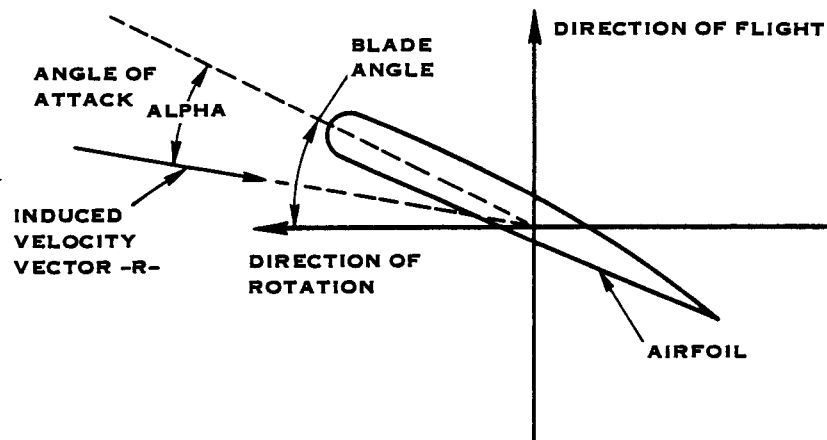


FIGURE 2. ANGLE OF ATTACK - ALPHA

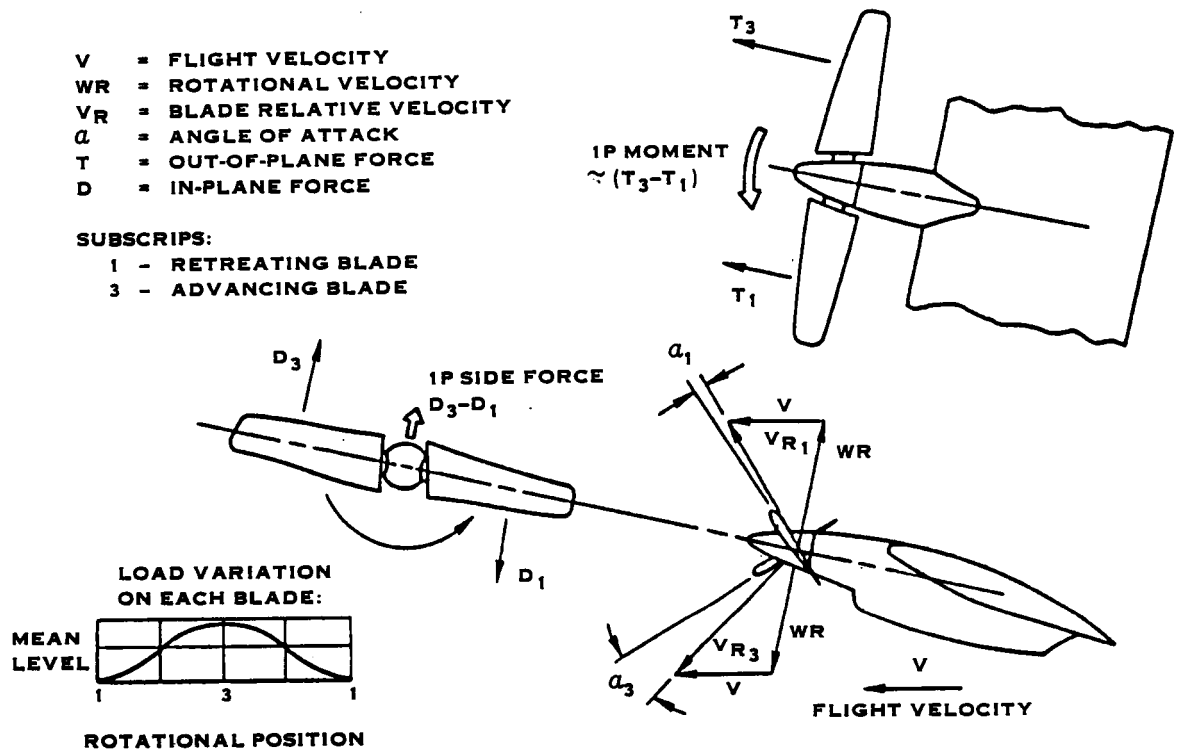


FIGURE 3. LOADING - AERODYNAMIC-CYCLIC

The major inertia load on the blade is the centrifugal load. It varies with the weight, mass center location and the square of the rpm of the blade. The centrifugal load acts along the blade axis and is considered a steady type loading.

As the air loads bend the blade, the mass center is deflected out of the rotational plane offsetting the centrifugal load causing a restoring moment which must be combined with the steady aerodynamic moment. The mass center can be deliberately be offset to alter the effective steady moment acting on the retention.

As the blade changes pitch out of the plane of rotation, part of the blade lies ahead of the plane and part behind. The centrifugal load acting on these two segments has a component of its load acting parallel but offset from the rotation plane. These two offset forces ahead and behind the plane produce a couple tending to twist the blade back into the rotation plane. This is the centrifugal twisting moment. This couple depends on the same factors as the centrifugal force. In addition the CTM varies with the sine of twice the blade angle. The CTM is considered to be a steady type loading. It is combined with the ATM to load the pitch change actuator system.

The pitch change trunnion roller on the butt end of the blade is a large offset distance from the retention bearing center. The twisting moment reactions on the trunnion roller produce offset moments which are included in the resultant steady bending moments.

A finite element model was used to analyze the blade. The aerodynamic pressures were applied as discrete loads at the nodes of the elements comprising the airfoil sections of the blade. The inertia loads were applied by rotating the mass model of the blade at the climb rotational speed about the Prop-Fan axis. The model was constrained at its inboard end. The blade retention and hub loads were derived from the constraint loads as forces and moments about an x, y, and z axis as shown in Figure 4. The loads were resolved in the plane of the blade retention ball bearing centers.

The aircraft climb condition has the highest flight vibratory loading and accumulates a large number of cycles over the life of the aircraft. The stress cycles accumulate at the rate of the Prop-Fan rotational speed. The climb condition therefore, was used for the design case and the retention loadings for the climb case are tabulated in Table I.

TABLE I. RETENTION LOADS

	<u>Fx</u> <u>Newtons</u> <u>(lbs)</u>	<u>Fy</u> <u>Newtons</u> <u>(lbs)</u>	<u>Fz</u> <u>Newtons</u> <u>(lbs)</u>	<u>My</u> <u>Newton-meters</u> <u>(in-lbs)</u>	<u>Mz</u> <u>Newton-meter</u> <u>(in-lbs)</u>
STDY + VIB	-368690 (-82890)	-35240 (-7922)	-14360 (-3229)	-3898 (-34499)	-2248 (-19893)
STDY - VIB	-368690 (-82890)	-29450 (-6620)	-2913 (-655)	1130 (10003)	-6449 (-57073)

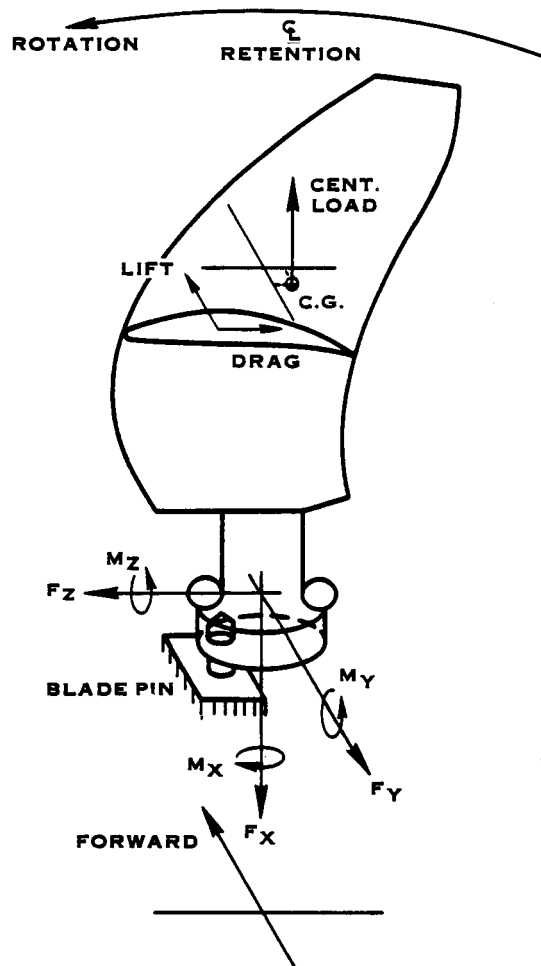


FIGURE 4. BLADE LOADING COORDINATE SYSTEM

The loads applied to the hub are identical to those applied to the retention. (Figure 5 shows a hub with its associated loads). However, in the past, it has been found that the side loads on the retention, notably the torque and thrust, have a negligible effect on the hub stressing. Therefore, the side loads are neglected in this analysis. The loads used in the hub analysis come directly from Table I and are tabulated in Table II below. Angular values refer to number of degrees clockwise from the direction of rotation looking tip to hub.

TABLE II. HUB LOADS

CENTRIFUGAL FORCE	368690 newtons (82890 lbs)
STEADY MOMENT (SBM)	4563 newton-meters @ 252 deg. (40385 in-lbs @ 252 deg.)
VIBRATORY MOMENT (VBM)	3104 newton-meters @ 144 deg. (27470 in-lbs @ 144 deg.)

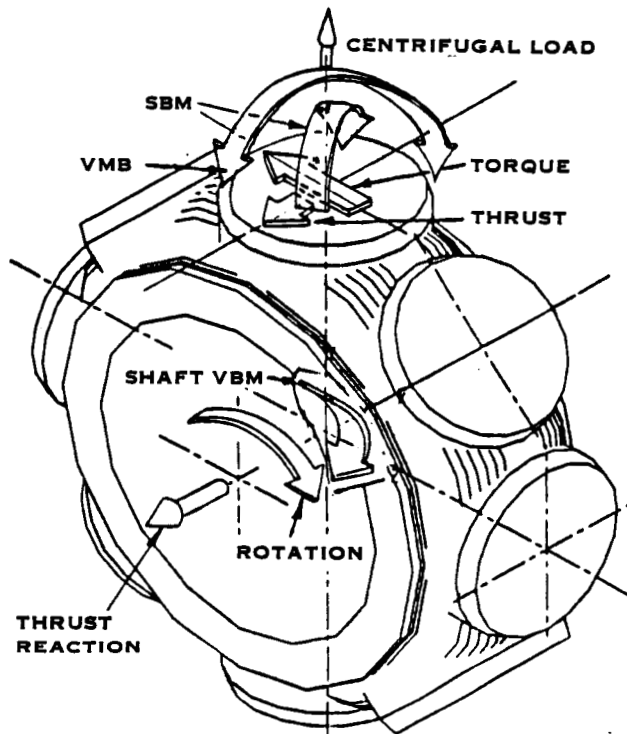


FIGURE 5. HUB LOADING

TAILSHAFT LOADS

The loads which are applied to the tailshaft can be broken down into five categories: thrust, torque, engine shaft/tailshaft preload, blade centrifugal load, and shaft bending moment. Because of its high impressed moment and large number of cycles, the aircraft climb condition once again was determined to be the design limiting case.

The thrust generated by the propeller and torque applied to the propeller are fed through the tailshaft. Therefore, the tailshaft must be able to withstand the 32,995 newtons (7,418 lbs) of thrust and the 25,165 newton-meters (222,700 in-lbs) of torque the engine produces. Only a small portion of the blade centrifugal load is transmitted to the tailshaft, the majority being absorbed by the hub. The engine shaft/tailshaft interface is made up of two cones seated in the hub and preloaded against each other by the propeller retaining nut through the engine shaft. This nut is torqued 3,390 newton-meters (30,000 in-lbs) producing a 298,906 newton (67,200 lb) axial preload on the cones. The moment load applied to the tailshaft is described in detail in the retention load section. This is a steady bending moment that produces once per revolution fully reversed bending stresses in the tailshaft because of its rotation. The moment magnitude is 8,645 newton meters (76,500 in-lbs).

All of the loads, excepting the engine shaft preload, are applied where the tailshaft and hub are joined. The preload is applied at the cone seats where the engine shaft and tailshaft interface.

BLADE RETENTION STRESS

The retention stresses were analyzed using a computerized analysis called H380. This analysis does a load balance on the bearing accounting for such parameters as number of balls, ball diameter, pitch diameter, forces, moments, material properties, and geometry. The results from this analysis that are used in retention design include Hertzian deflection and stresses, position of the ball contact pattern, and moment spring rate as illustrated in Figure 6. For the loads listed in Table I, the following retention design goals have been achieved: unlimited life ($>10^8$ cycles) for high cycle fatigue (HCF) and a low cycle fatigue (LCF) life of 10,000 cycles as illustrated in the normalized Goodman diagram in Figure 7. The predicted low cycle fatigue life of 10,000 cycles is less than the desired 50,000 cycles. The 10,000 cycle life is equivalent to 10,000 excursions from rest to 100% rpm or to 2500 pitch change cycles. This application will probably see less than 500 pitch change cycles or on-off cycles. This gives a five to one pitch change life factor or a twenty to one on-off life factor. The ball patterns are on the race for all flight conditions.

In addition to the Hertzian stress calculations for the ball race interface, the subsurface shear stresses were also calculated using another computerized analysis called P248. This calculation insures that the hardening depth exceeds the expected peak of the subsurface shear. Figure 8 shows the depth characteristics of the carburizing process, and in Figure 9, the subsurface shear steady and cyclic stresses are plotted verses depth. The specified depth of .104 cm (.041 inches) for the fully hardened zone 59 Rockwell C minimum is sufficient to envelope the peaks in Figure 9. Figure 10 shows the crossover between the core material 34 Rockwell C allowables and the subsurface shear which indicates a minimum depth of hardening of .297 cm (.117 in.). The carburizing depth is defined as the point where the hardness is equal to the core value of 34 Rockwell C. The 50 Rockwell C equivalent depth is specified as .103 cm (.08 in.) to .254 cm (.1 in.). This is 2/3 of the full depth or .3 cm (.12 in.) min, and will insure that the hardness does not decrease to the core value above the minimum depth of .297 cm (.117 in.).

As a further criterion of the retention design, the centrifugal load, using H380, was increased to 150 and 200 percent of the nominal. At 150 percent overspeed (the stress is plotted on Figure 7 as 150%cf), the retention balls and races were found to have no additional permanent deformation than the acceptable value of .00005 in./in. of element diameter. At 200 percent overspeed the force on the balls was enough to cause greater permanent deformation. This deformation, however, will not cause a catastrophic failure in the retention system and meets the overspeed design requirements.

~~DO NOT WRITE IN THESE SPACES~~

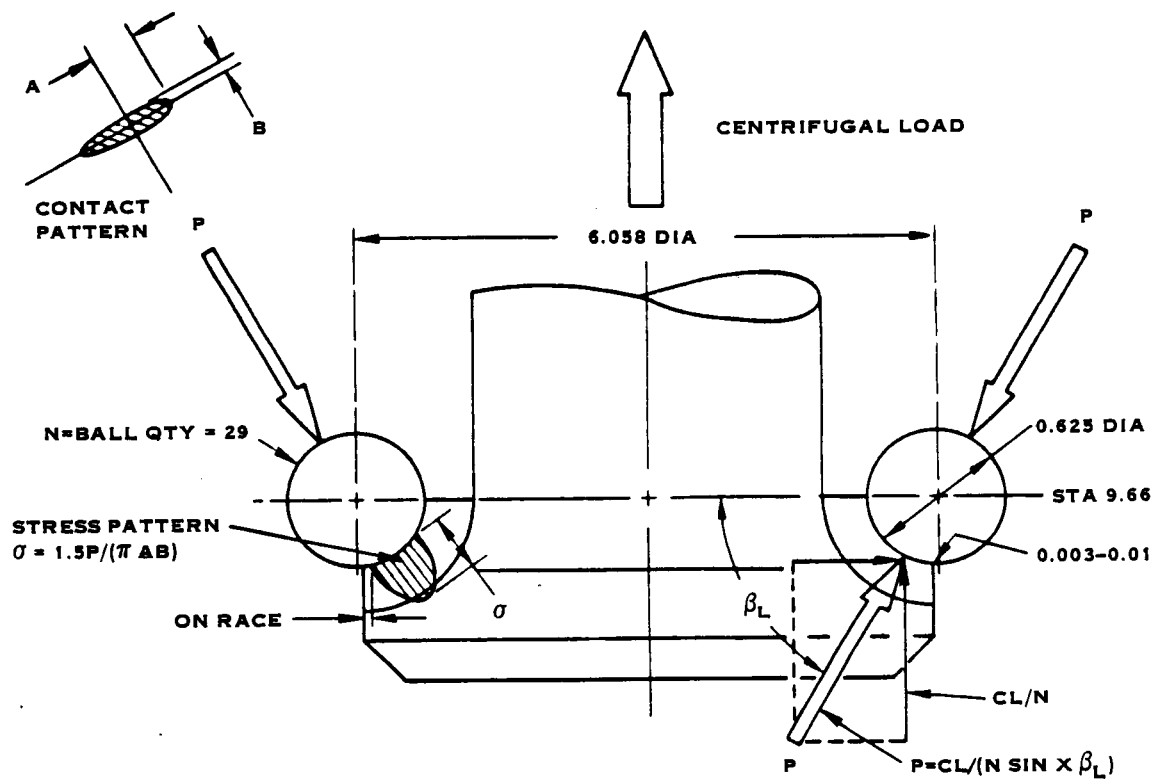


FIGURE 6. RETENTION

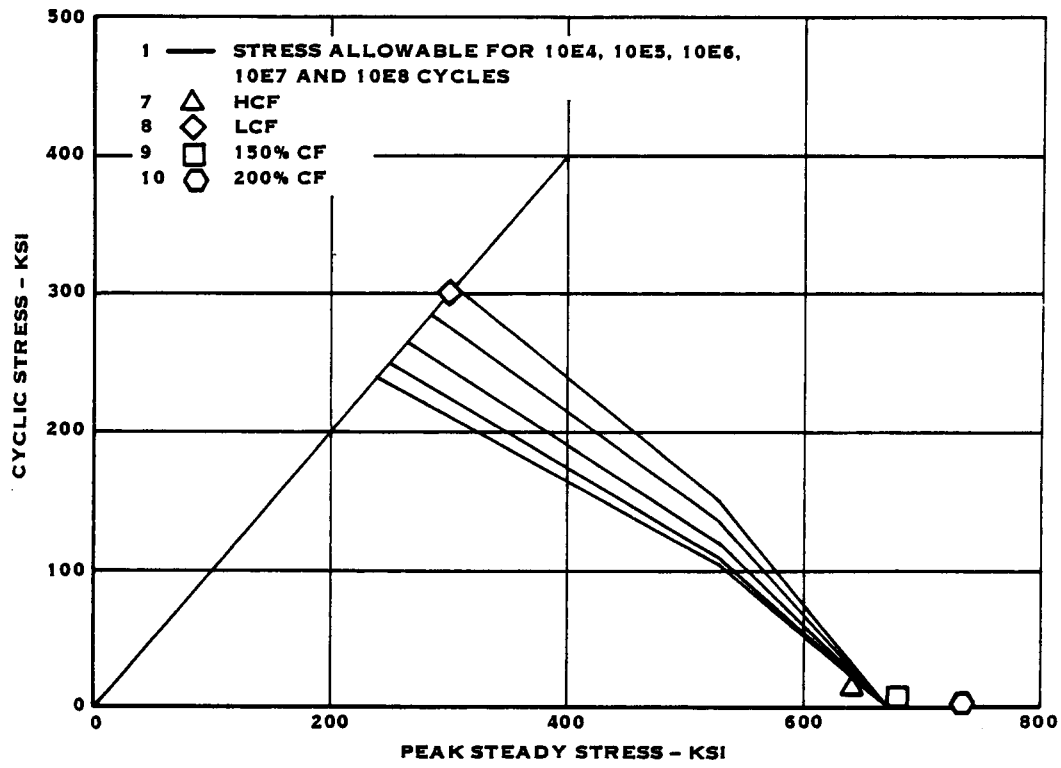


FIGURE 7. BLADE BEARING STRESS CRITERIA

ORIGINAL PAGE IS
OF POOR QUALITY



FIGURE 8. RACE HARDENING

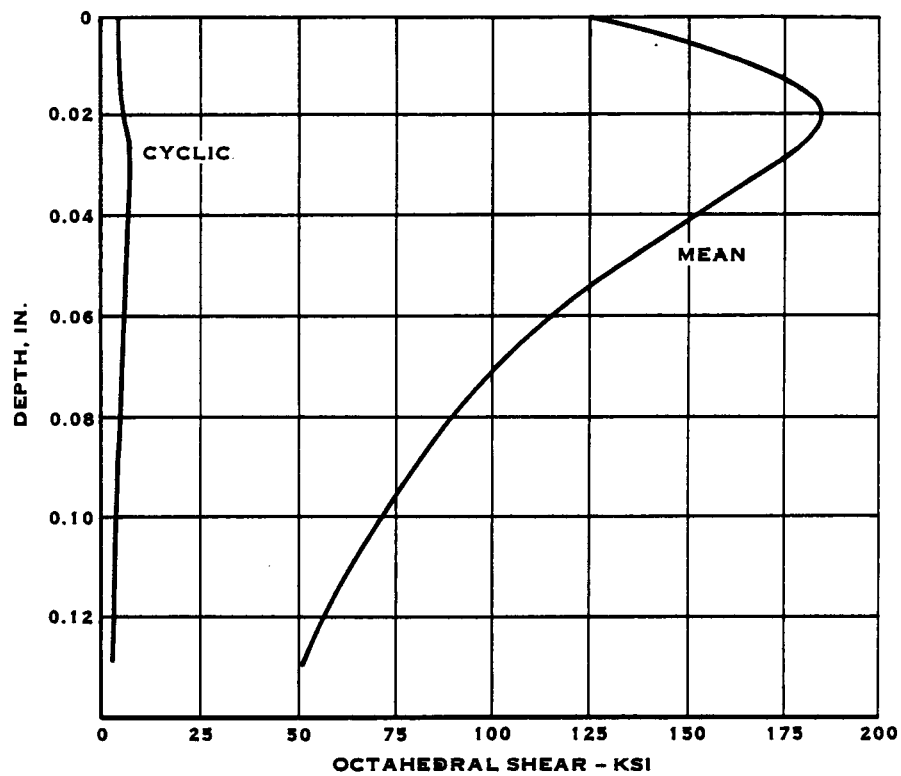


FIGURE 9. SUBSURFACE RACE STRESS

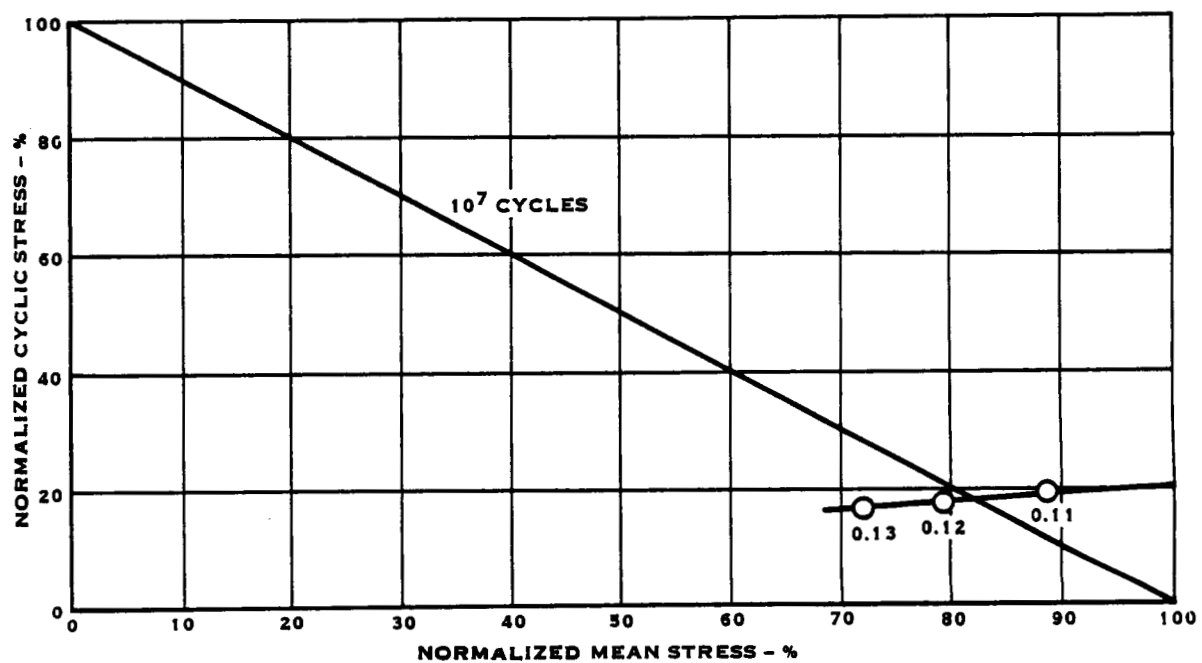


FIGURE 10. RACE AND BALL STRESS CRITERIA SUBSURFACE OCTAHEDRAL SHEAR STRESS

BARREL STRESS

The stress analysis of the barrel is done by splitting it into three sections; the front ring, the rear ring, and the barrel arms. The front and rear rings are analyzed separately using a computerized analysis called Ring-28. For this eight bladed propeller the barrel was split into six equal segments over the 22.5 degrees necessary to provide mirror symmetry (See Figure 11). Each segment is a planar cross section cut from the center line of the propeller radially outward. The center of gravity, area, and moment of inertia for each slice is computed for the front and rear rings (See Figure 12 and 13). These cross sectional properties, which vary with their azimuthal position, are then used to construct the ring. The loads, which originate in the barrel arms, are transposed to radial and tangential forces at the sections on the ring using shear flow and Wise coefficients'. The stresses can then be calculated for the inner and outer surfaces of the front and rear rings.

The barrel arms are analyzed using a shell of revolution computer analysis called H727. Since the cross section must be constant, to be conservative, the thinnest section of the arm is used in the model (See Figure 14). The steady and vibratory bending moments, input as equivalent axial loads, and the centrifugal force, an axial force, are applied at the hub raceway to obtain the effect secondary bending through that section.

For the top of the barrel arm, the hoop stress from Ring-28 is added to the hoop stress for the same position from H727 to obtain an effective combination of the two loading patterns at that point (See Figure 11). Another relatively high stressed point from the analysis is just below the ball bearing. These two worst stress points are plotted on the Goodman diagram in Figure 15. The amount that the point is below the line on the Goodman diagram indicates how much extra strength the part has.

Barrel stressing was also analyzed using 3D finite element analysis, the results of which are summarized in Appendix A.

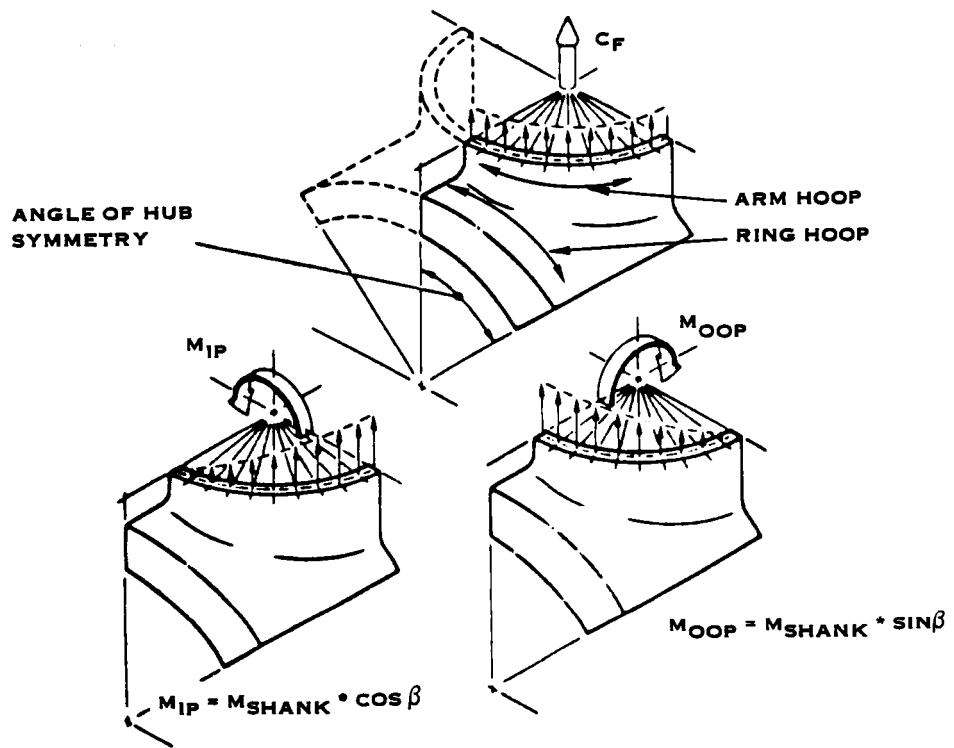


FIGURE 11. HUB - LOAD RESOLUTION

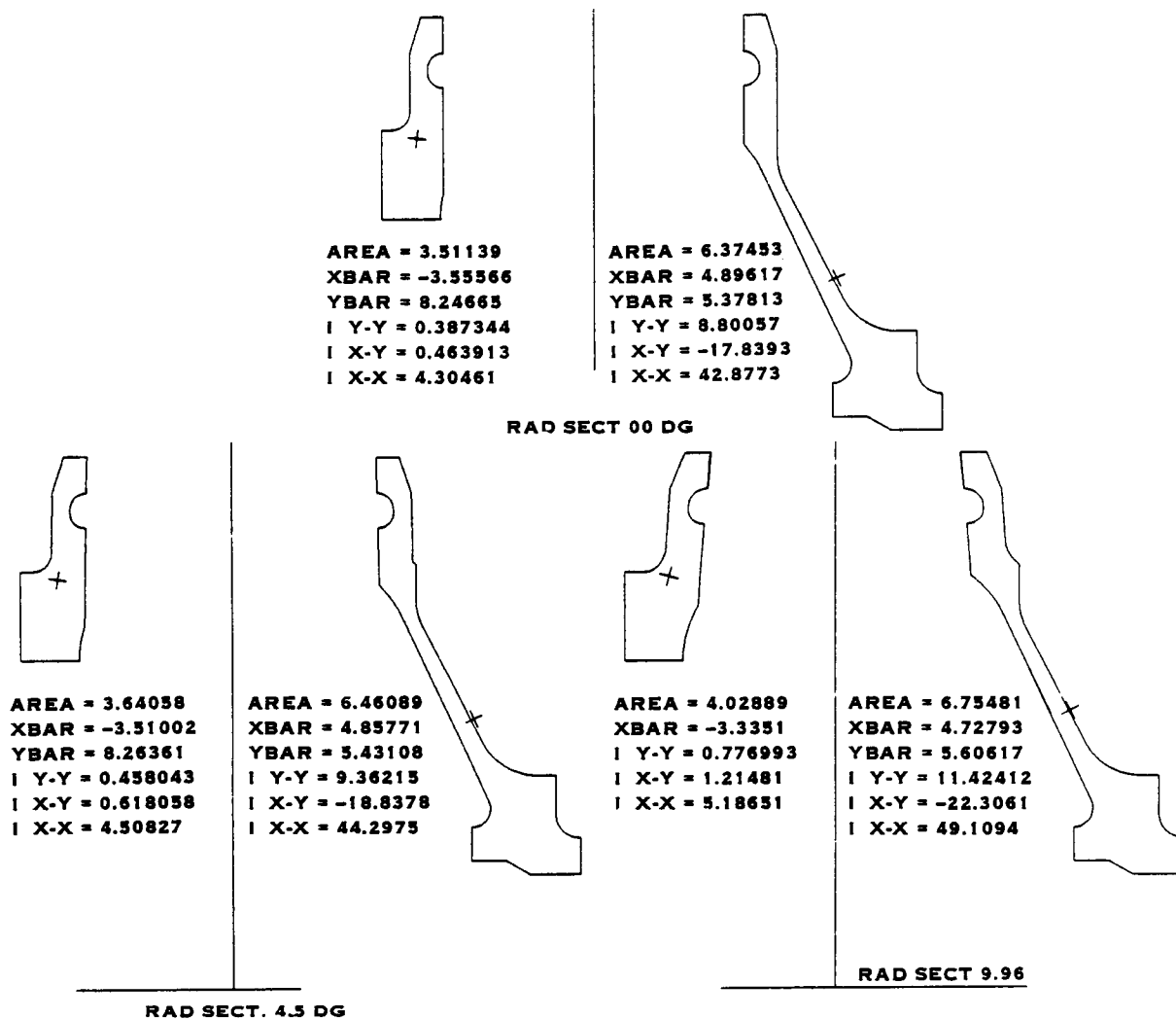


FIGURE 12. RING SECTION PROPERTIES

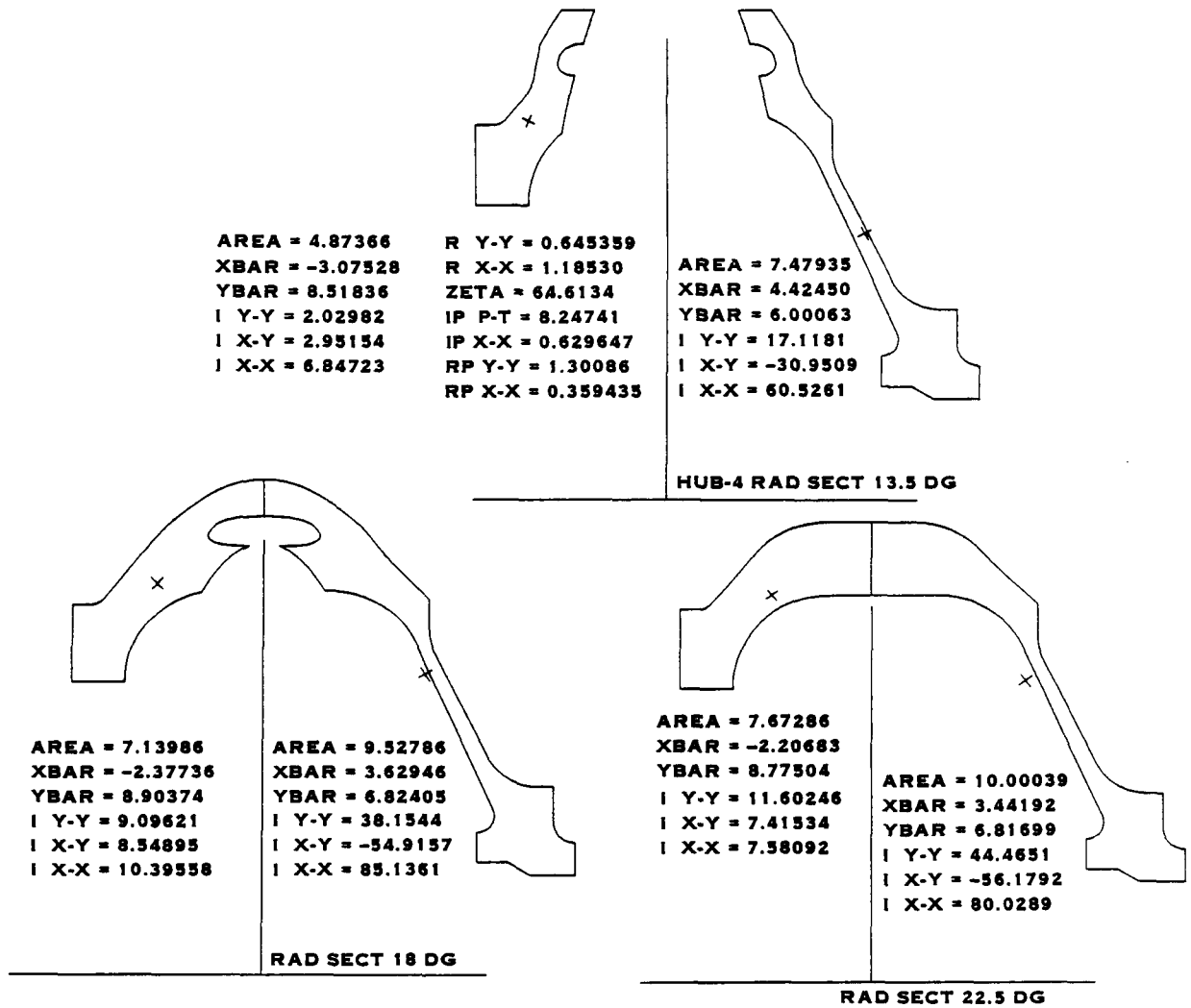


FIGURE 13. RING SECTION.PROPERTIES

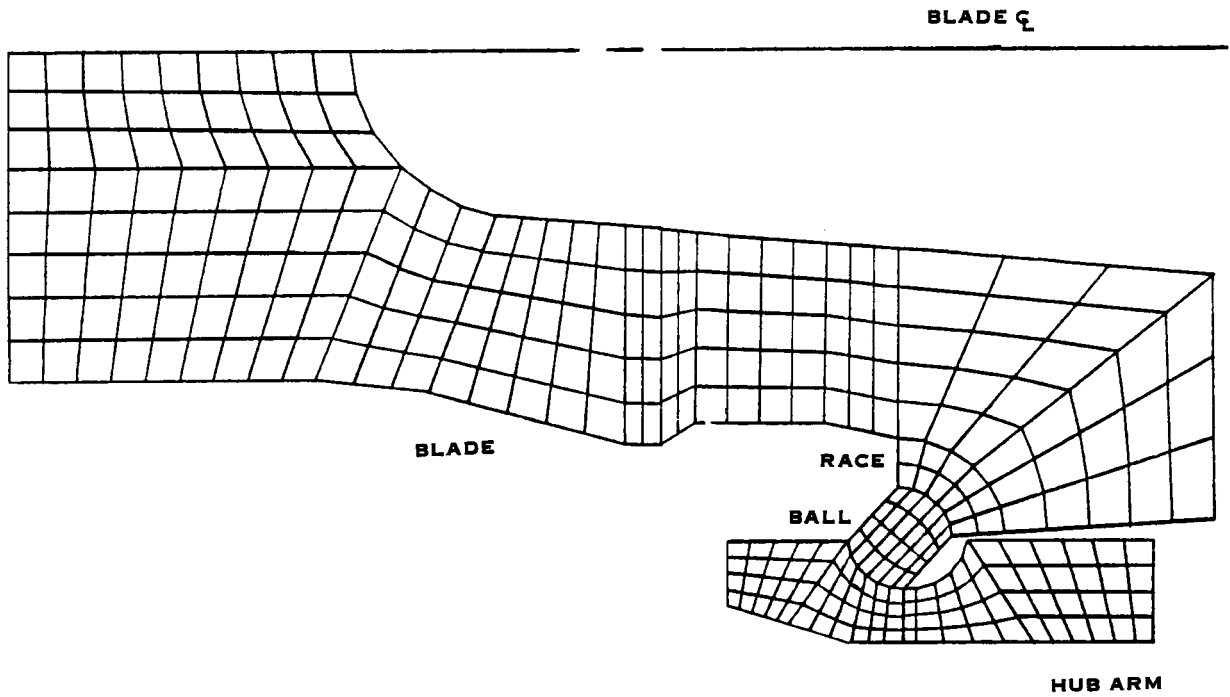


FIGURE 14. BLADE RACE, HUB ARM MODEL

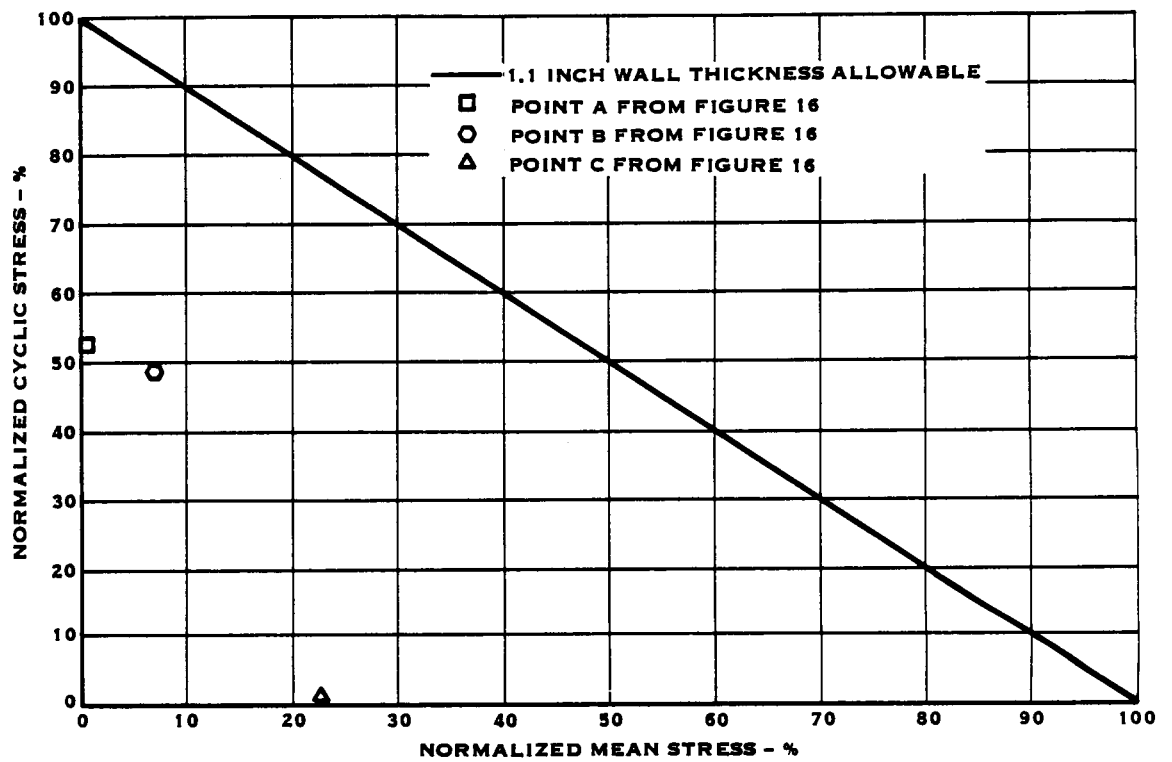


FIGURE 15. RING AND ARM STRESS CRITERIA MACHINED SURFACES

TAILSHAFT

The tailshaft was analyzed using a shell of revolution computer analysis called H746. A radial deflection, due to centrifugal load of .035 cm. (.0014 in.) was calculated for the vicinity of the tailshaft. The tailshaft model was then predeflected by this amount to reproduce the effect of its share of the centrifugal load. The remaining loads, as explained earlier in the tailshaft load section, were applied to the nodes of the model and the stresses calculated are shown in Figure 16 and on the Goodman diagram shown in Figure 17.

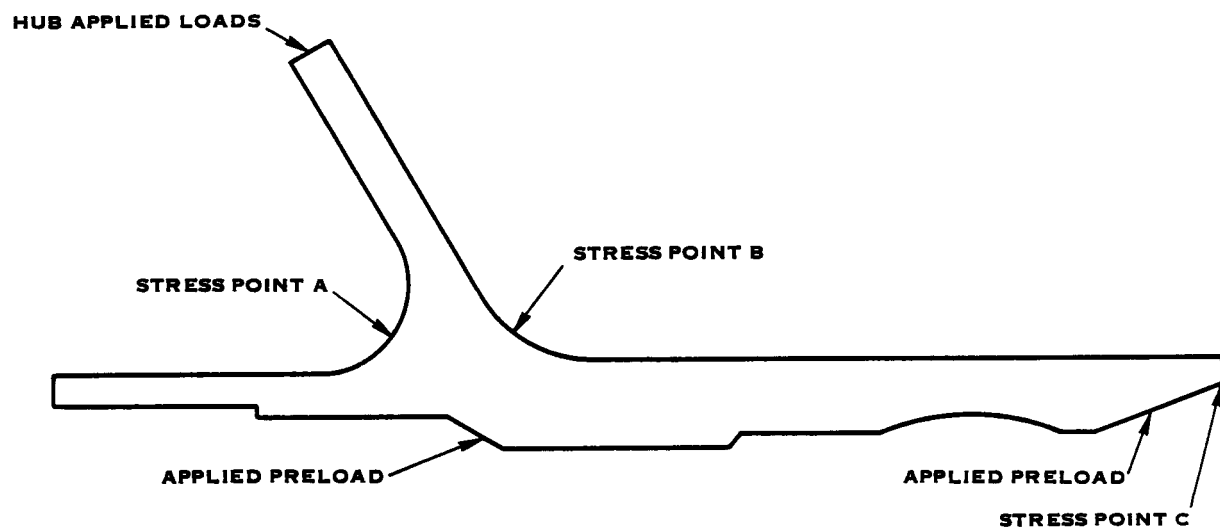


FIGURE 16. TAILSHAFT MODEL

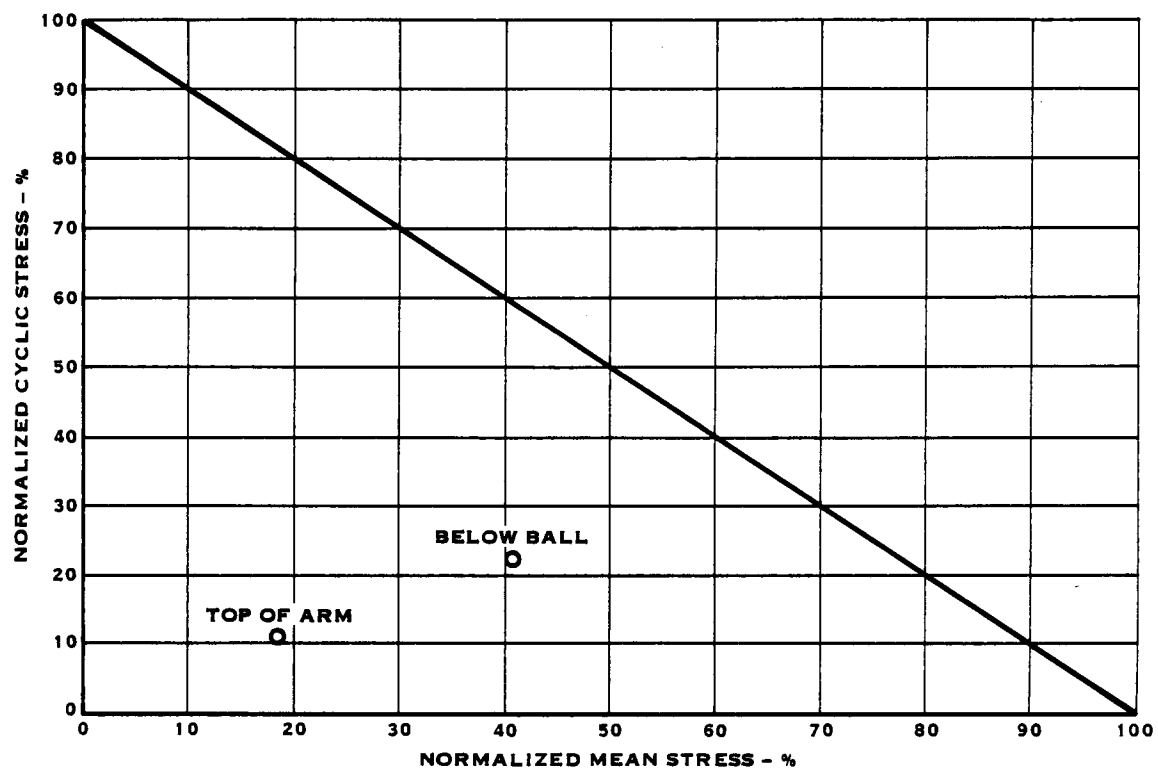


FIGURE 17. TAILSHAFT STRESS CRITERIA

SPRING RATE

The stress levels in the previous sections are well below allowables indicating that there is adequate stress margin. Obviously stress was not the sizing criterion for the hub assembly. Hub wall thickness is dictated by a required retention moment spring rate or stiffness. The blade, because of the more rigorous geometric constraints put on it, has a spring rate and mass distribution of its own which usually cannot be varied to any extent without upsetting the delicate balance between stresses and loads. Therefore, one of the major functions of the hub assembly is to provide a retention stiffness that will place the natural frequencies of the propeller outside the restricted range (shaded regions of Figure 18).

The first, second, and third modes shown on Figure 18 are the first three blade natural frequencies. The hub in-plane and out-of-plane spring rates (nominally 13.7 and 15.5 million in.-lbs respectively) are plotted on these mode lines. The natural frequencies of the propeller system for these points are outside the various indicated excitation frequencies and their tolerances (10% on two excitations per revolution - 2p, 7.5% on three excitations per revolution - 3p, and 5% on four excitations per revolution - 4p). Therefore, the hub in-plane and out-of-plane spring rates are acceptable for this propeller assembly.

The spring rate of the hub assembly is divided into components which are evaluated separately for ease of analysis. These are: the blade shank, blade/race interface, race, ball, barrel arm, barrel bridge (affects inplane only), and barrel rings. These series springs are summed reciprocally to produce a total hub spring rate.

The finite element shell of revolution model of the blade shank, race, and barrel arm sections provided both the stress and the stiffness values (See Figure 14) by computer analysis called H727. The rotation in each of the above mentioned parts is found for a given moment load and a spring rate is calculated by dividing the moment by the rotation. The ball, modeled as a rigid link in this analysis, to serve as part of the load path, has a non-linear spring rate whose stiffness is calculated by computer program called H380.

The bridge consists of the hub material in between the barrel arms and thus its spring is effective only in the inplane direction. The hub, as shown in Figure 19, is cut by planes passing through the y axis between 45 and 135 degrees from the forward direction by a three dimensional computer aided design program called CATIA. The section properties are calculated for each slice (Figure 20 and 21). A graph of these section properties vs. distance along the bridge is constructed (Figure 22), and a Nastran finite element model using beam elements is formed. A simulated moment is applied to the model, rotations are found and the spring rate is calculated.

Barrel stiffness was also analyzed using 3D finite element analysis methods, the results of which are summarized in Appendix A.

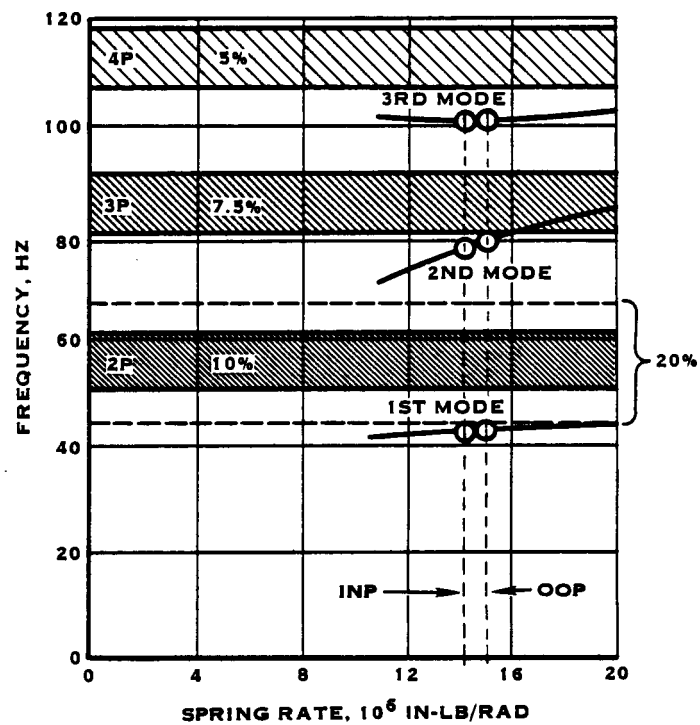


FIGURE 18. PROPELLER FREQUENCIES VS. TOTAL HUB SPRING RATE

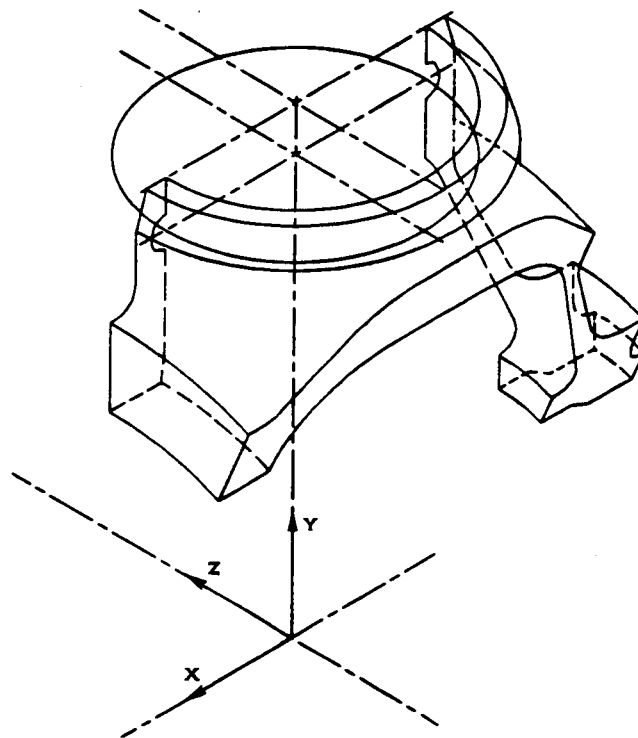


FIGURE 19. HUB SEGMENT



AREA = 2.81930
XBAR = -2.90985
YBAR = 9.16975
I Y-Y = 0.407504
I X-Y = 0.158783
I X-X = 1.46342

HUB SECT 45 DG



AREA = 2.33717
XBAR = 9.27361
YBAR = 3.08569
I Y-Y = 1.12204
I X-Y = -0.073189
I X-X = 0.249207

HUB SECT 54 DG



AREA = 1.67715
XBAR = -3.31605
YBAR = 9.39278
I Y-Y = 0.098251
I X-Y = 0.002335
I X-X = 0.783310

HUB SECT 72 DG

FIGURE 20. BRIDGE SECTION PROPERTIES



AREA = 2.23470
XBAR = -3.09031
YBAR = 9.32103
I Y-Y = 0.239029
I X-Y = 0.088684
I X-X = 1.00111

HUB SECT 126 DG



AREA = 1.67715
XBAR = -3.31603
YBAR = 9.39256
I Y-Y = 0.098297
I X-Y = 0.001251
I X-X = 0.789078

HUB SECT 108 DG



AREA = 2.56543
XBAR = -2.91533
YBAR = 9.26060
I Y-Y = 0.370034
I X-Y = 0.192150
I X-X = 1.17827

HUB SECT 135 DG

FIGURE 21. BRIDGE SECTION PROPERTIES

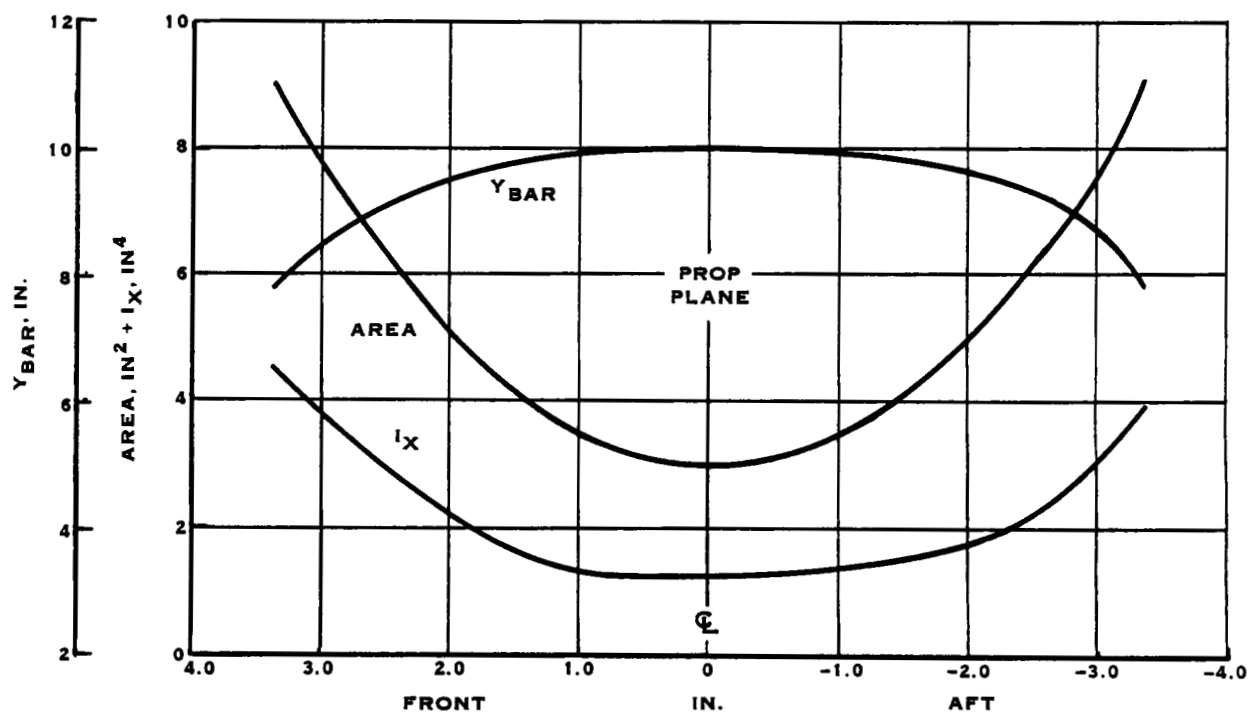


FIGURE 22. HUB ARM BRIDGE SECTION PROPERTIES

The blade/race interface also has a spring associated with it. These two parts are loaded against each other by the pressure of the bearing causing Hertzian deflection between them. Approximating this condition by a cylinder in a groove, rotations can be calculated for the applied moments and a spring rate can be found.

The barrel rings are another spring that goes into making up the total hub spring rate. Their deflection which make up the rotation due to applied moments is part of the analysis done to calculate the stresses by computer analysis called Ring-28. The rings are loaded differently by inplane and out of plane moments, so, the spring rates are slightly different in the two directions.

The last spring to be covered is the ball bearing which can readjust its contact angle under load and exhibit relatively large Hertzian deflections. This behavior makes its spring rate the smallest in magnitude and thus the most important. Because the individual spring rates are added reciprocally, the smallest sets the maximum limit for the total spring rate and as the larger individual springs are added to it the total hub spring rate becomes smaller. By adjusting the bearing geometry, the ball spring rate can be varied quite substantially to obtain an acceptable total spring rate. Figure 23 shows a survey of retentions, analyzed on our H380 bearing analysis, that were considered for this application. Off race indicates the ball race contact pattern edge is off the race at some loading condition and indicates unsuitability due to a reduction in capacity. The bearing chosen has twenty nine 1.588 cm. (.625 in.) diameter balls in a 15.392 cm. (6.06 in.) pitch diameter.

Figure 24 shows a tabular listing of all the spring rate values and also the total hub assembly spring rate value. This spring rate value can then be added to the blade model and the natural frequencies of the whole propeller system can be calculated for the different blade modes. These values are plotted for the inplane and out of plane directions in Figure 18. This shows the predicted natural frequencies to be out of the range of the anticipated exciting forces.

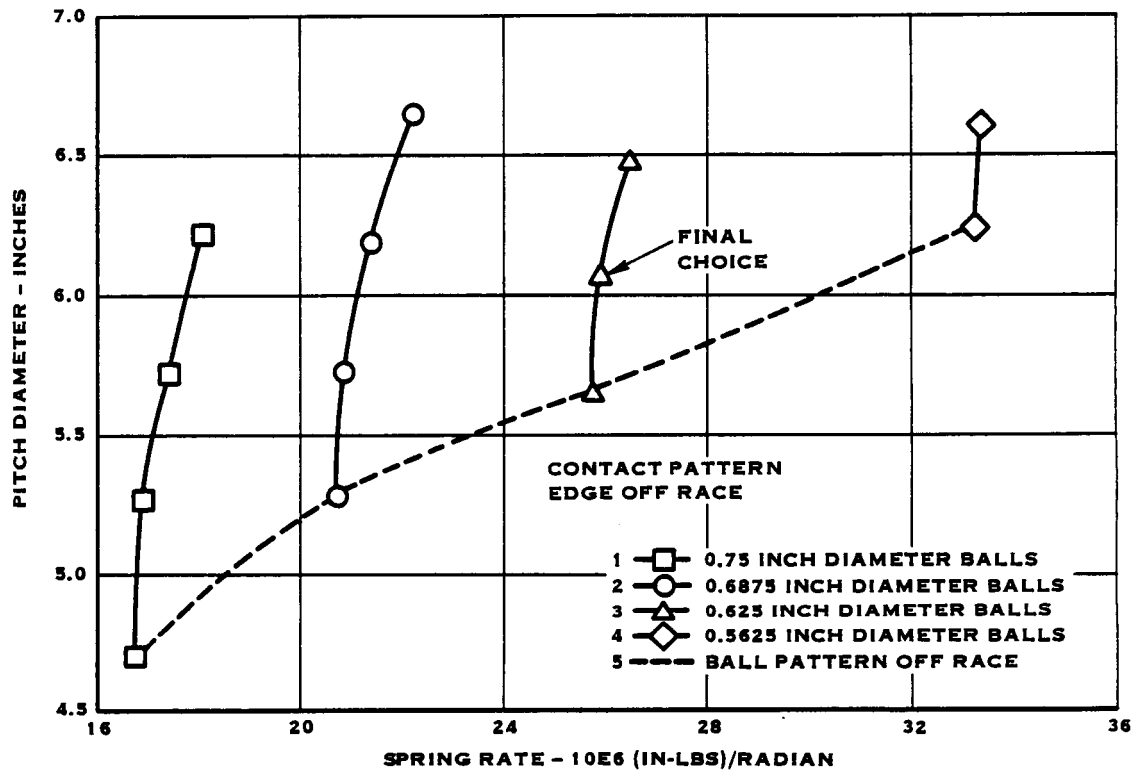


FIGURE 23. BEARING O.D. VS. SPRING RATE

	<u>IN PLANE</u>		<u>OUT OF PLANE</u>	
BLADE	165		165	
BLADE/RACE	217		217	
RACE	876		876	
BALL	26.1	29.2	26.1	29.2
BARREL ARM	675		675	
BARREL BRIDGE	370		—	
BARREL RINGS	71		67	
TOTAL, K_T	13.27	14.03	15.04	16.03

$$K_T = 1 / (1/K_1 + \dots + 1/K_N)$$

FIGURE 24. HUB SPRING RATE IN * LB/RAD * 10⁶

WEIGHTS

The weight breakdown for the hub assembly parts appears in Figure 25.

	<u>POUNDS/PROP</u>
HUB	218.6
RET.	
BLADE/RACE	4.48
BLADE SEAL	2.08
BLADE RING	16.20
BALL (232)	8.4
BALL SEPARATOR	0.80
FRICTION STRIP	0.16
	<hr/>
	32.12
TOTAL	250.8

FIGURE 25. HUB AND RETENTION WEIGHT

CONCLUSION

The hub assembly meets all design requirements. All components will meet or exceed life expectations. The single exception is the retention bearing low cycle fatigue life which is predicted to be less than 50,000 cycles but will exceed the anticipated utilization by a twenty to one factor.

HA
~~INTENTIONALLY BLANK~~



REFERENCES

1. Niles and Newell, Airplane Structures, John Wiley and Sons, Volume II, Third Edition, January, 1946.

APPENDIX A
HUB RETENTION STIFFNESS AND STRESSING
3D FINITE ELEMENT ANALYSIS

Introduction

A 3D finite element analysis of the LAP barrel was performed to verify the retention stiffness and barrel stressing for centrifugal, 2P and 1P loading conditions. Solution accuracy checks on model mesh size and constraints were also made. The following sections summarize the FEA results and compares the FEA results with the ring analysis.

Conclusions

1. The FEA in-plane (IP) barrel stiffness is 37×10^6 in-lb/rad. The out-of-plane (OOP) barrel stiffness is 70×10^6 in-lb/rad.
2. The FEA IP stiffness is 33% lower than the stiffness obtained from the ring analysis. The FEA OOP stiffness is 15% higher than the ring analysis.
3. Stress levels obtained for all the FEA load cases are below the allowables.
4. The barrel stiffness is not sensitive to the model ball load application point.
5. For the 2P moments of 10,000, 20,000 and 28,000 in-lbs. the IP retention stiffness decreased a maximum of 3%. The OOP stiffness increased only .3%.
6. In this analysis, the 8-noded brick finite element model is adequate for determining barrel stiffness and stressing.

Methodology

F. E. Model: Structural symmetry permitted the modeling of only one-sixteenth of the barrel; see Figure A1. The model consists of 251 8-noded (8N) CHEXA and six-noded (6N) PENTA solid elements.

The mesh density around the barrel arm was defined so that a race node would represent a ball center. Nominal dimensions were used to construct the model.

To prevent rigid body motion, the end of the barrel tailshaft, which butts up against the thrust face of the engine, was rigidly fixed. The boundary conditions on the symmetry faces of the barrel are automatically set in the cyclic symmetry solution sequence to reflect the applied load condition.

Loading

Sinusoidal ball load and bearing race contact angle distributions were obtained for each load case using the Nonlinear Single Race Retention Stiffness Analysis Program F264CL and a Fortran program. Unlike current 3D FEA barrel analyses in which the ball loads were distributed over several nodes at each ball center location, the ball loads in this analysis were applied to a single race node at each ball center location; see Figure A2. This method of loading recognizes that the mesh density in the race area is too coarse to approximate the Hertzian ball load distribution and that the local "deflection" footprinting effect is negligible. This was verified by running a case with two loaded nodes. Asymmetric arm loadings for 2P and 1P modes are accounted for by using the Dihedral Cyclic Symmetry solution format in MSC/NASTRAN.

Stiffness

In- and out-of-plane retention stiffness values are obtained by performing a series of applied load iterations on the barrel. These iterations are necessary due to the nonlinear action of the barrel under load. The iteration process starts by initially applying a uniform load distribution with a constant contact angle to the raceway. Axial and radial displacements are obtained at the top, bottom, in-plane left and right locations on the race at the appropriate contact angle; see Figure A3. Compliances are then calculated at these points. These compliances are added to the blade, blade/race, race and ball without the kinematics, are input into F264CL to represent the entire retention flexibility. The kinematics are included in F264CL. This results in a new load distribution which is then applied to the FEA model. The process continues until two consecutive iterations result in compliances which are within 5% of each other. In- and out-of-plane cocking angles are then obtained from F264CL and converted into retention moment stiffnesses.

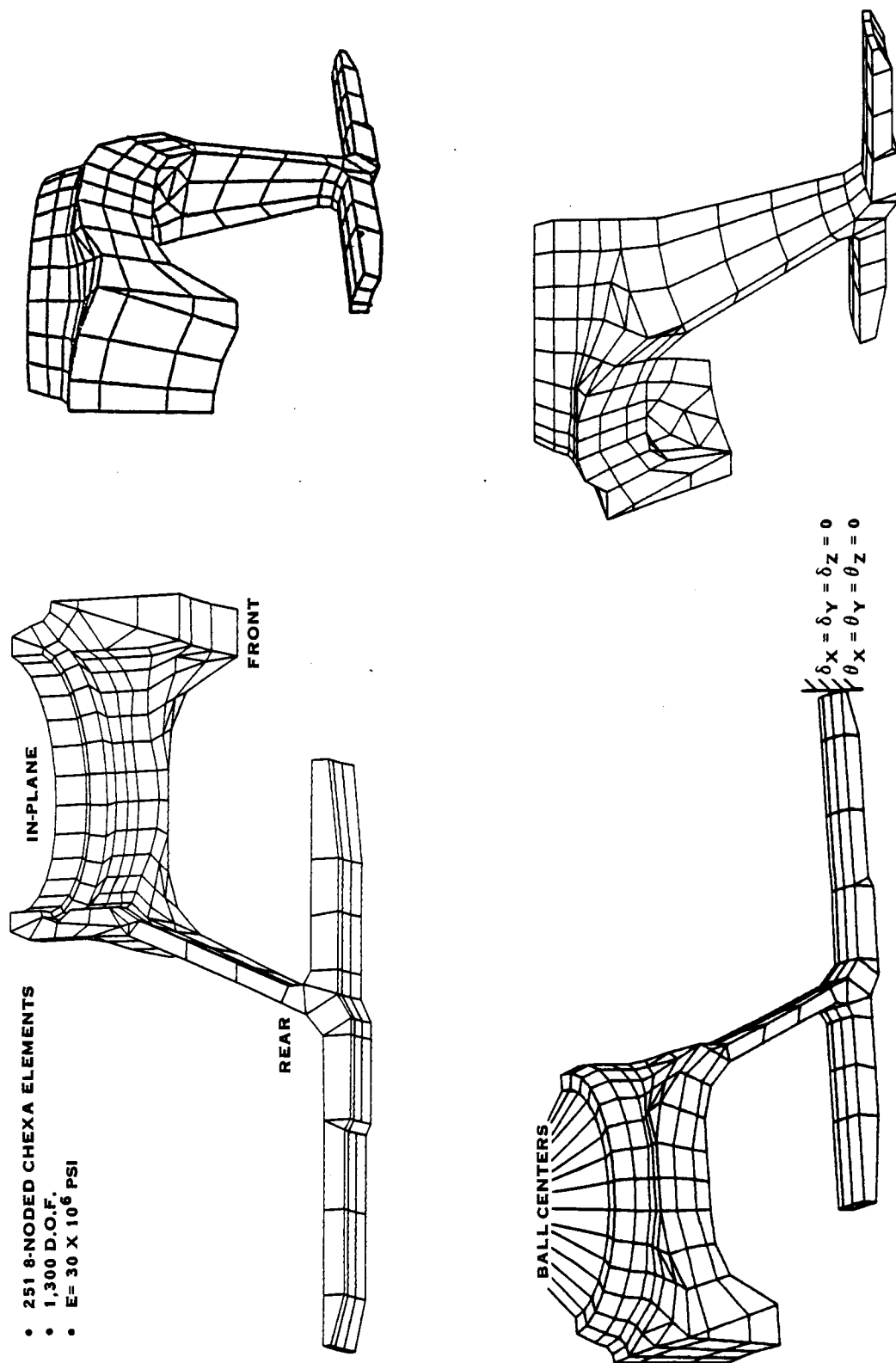


FIGURE A1. 3-D FINITE ELEMENT MODEL -- 1/16 SEGMENT

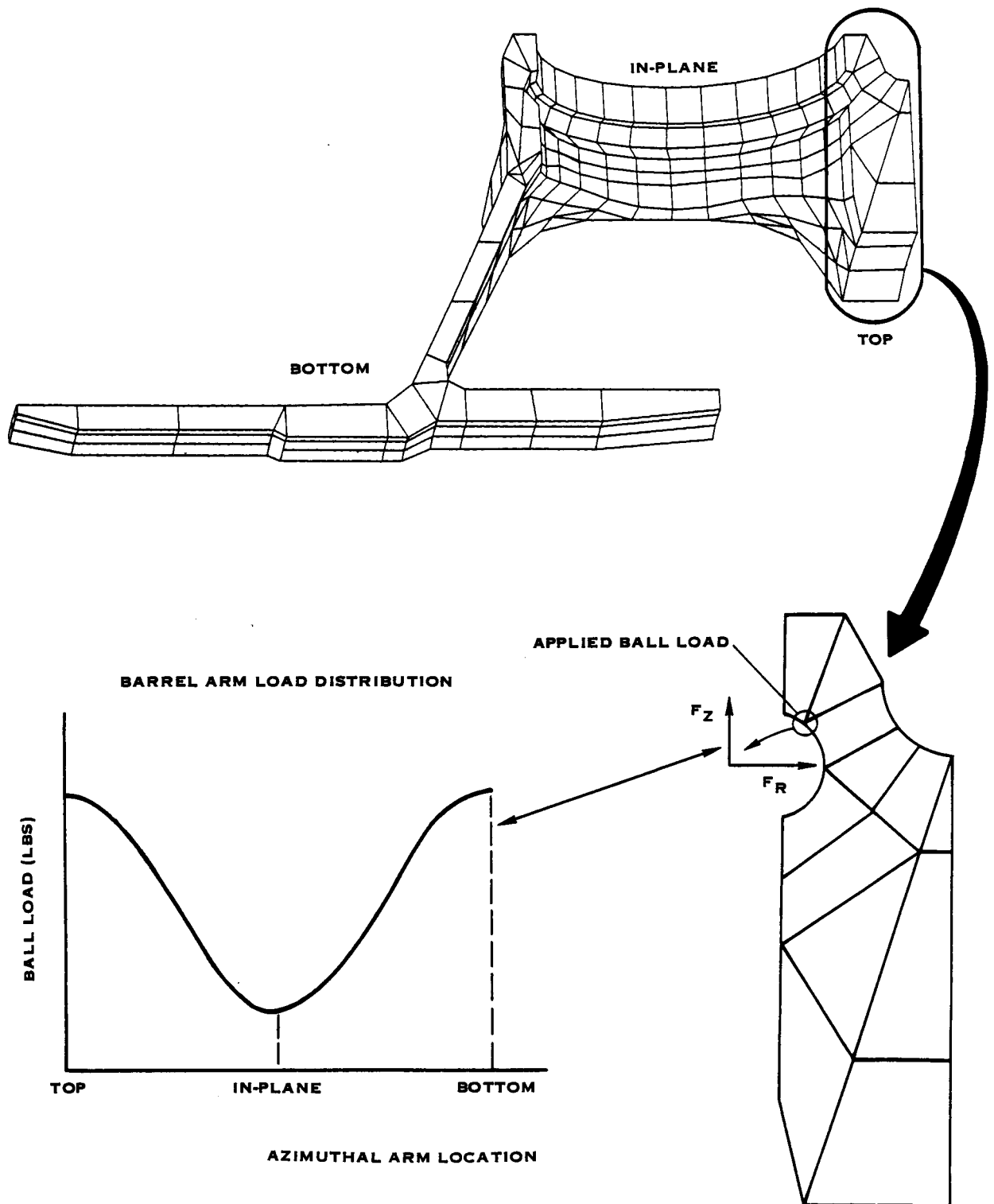


FIGURE A2. MODEL LOAD APPLICATION

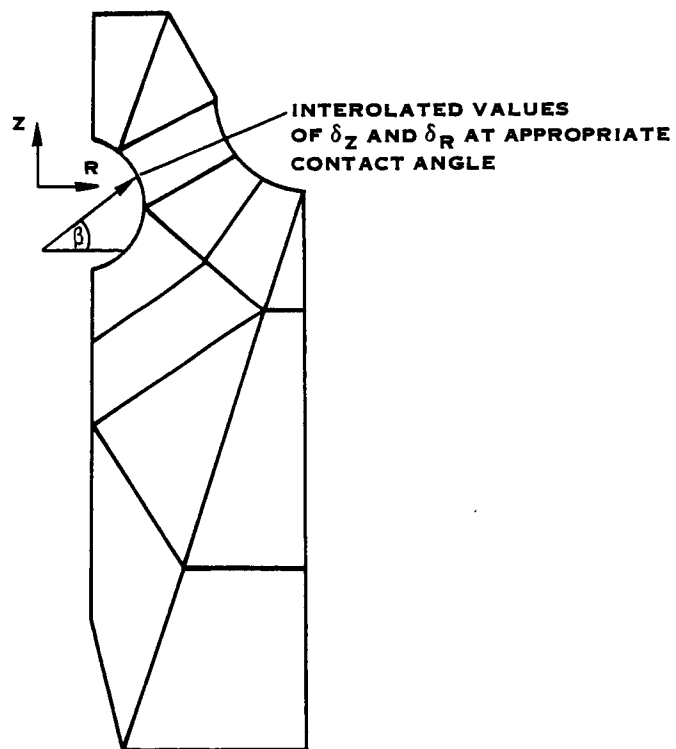
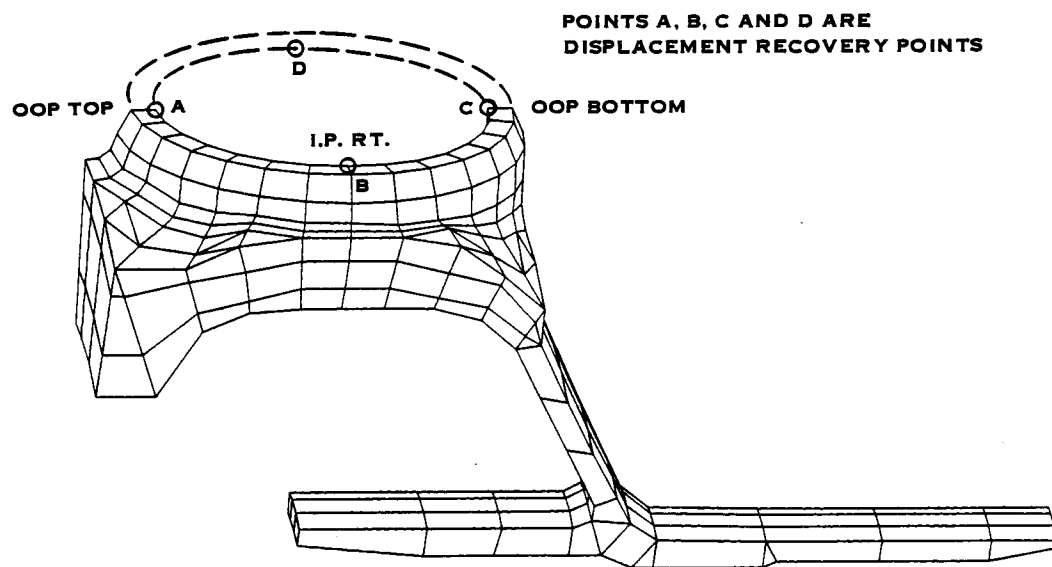


FIGURE A3. DATA RECOVERY POINTS FOR STIFFNESS ITERATION PROCESS

Analysis

Stiffness Results: A centrifugal force of 86,000 lbs. was applied to the model. This load application resulted in an in-plane retention stiffness (IP) of 10×10^6 in-lb/rad. and an out-of-plane retention (OOP) stiffness of 18×10^6 in-lb/rad. From these values in- and out-of-plane barrel stiffness terms are obtained and further reduced down into their fundamental components of the ring, arm and bridge to determine relative component stiffnesses; see Figure A4. The bridge is the softest spring in the barrel. The magnitude of these stiffnesses, however, are approximate in that assumptions are made where the arm ends and the ring begins; see Figure A5.

A comparison between the FEA and the ring analysis is shown in Figure A6. Differences between the two approaches are primarily due to the use of a sinusoidal load and contact angle distribution in the finite element analysis.

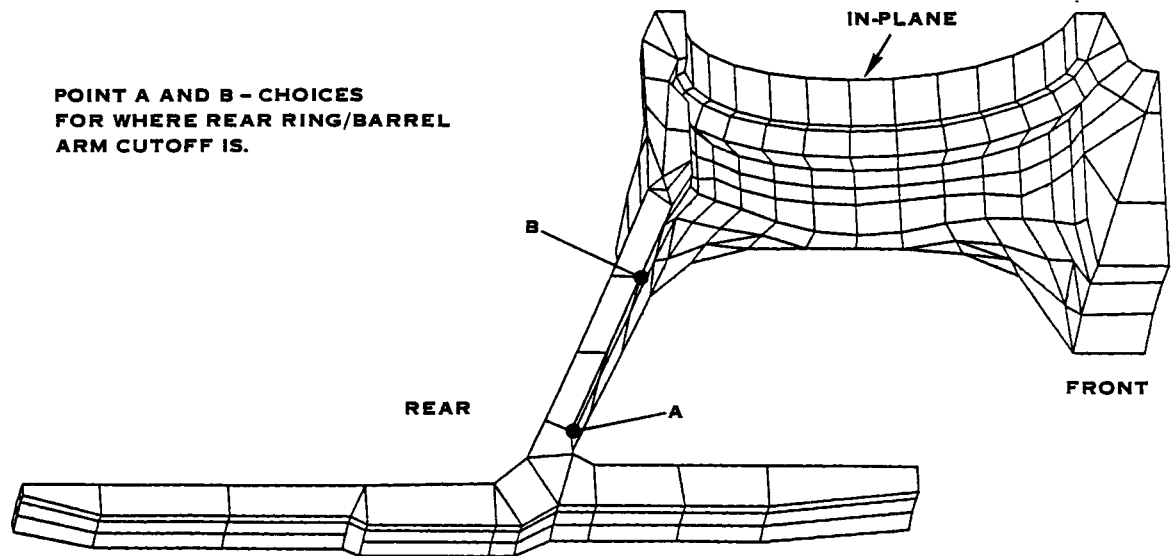
The 2P bending retention stiffnesses were obtained for a centrifugal force of 86,000 lbs. plus 10,000, 20,000 and 28,000 in-lb. vibratory moments. For each load case, the applied moment was split into IP and OOP components where the resultant moment was oriented at the calculated IP bending mode orientation of $\phi = 142^\circ$; see Figure A7. This orientation represents a flatwise bending on the blade. A summary of the IP and OOP bending retention stiffnesses are shown in Figure A8. An arm load phasing of .707 on each arm was found to produce the lowest barrel stiffness and highest stresses. For the range of applied moments, the IP and OOP stiffnesses changed a maximum of 3% and .3% respectively. Based on this result, it is assumed that inclusion of the steady bending moment would not significantly reduce the retention stiffnesses.

In- and out-of-plane retention stiffnesses for the centrifugal force and 2P cases are plotted in Figure A9 for the purpose of obtaining flatwise and edgewise retention stiffness values for the 2P case. The edgewise and flatwise retention stiffnesses on the centrifugal force only line were obtained by calculating barrel compliances at points A, B, C and D which lie on the edgewise-flatwise axes and following the load and stiffness procedure previously described. A curve was fit to the four points. A similar curve was assumed for the 2P data. A flatwise retention stiffnesses of 11×10^6 in-lb/rad. and an edgewise retention stiffness of 13.5×10^6 in-lb/rad. are obtained from this procedure.

A IP flatwise loading retention stiffness was also obtained for a centrifugal force of 86,000 in-lb. and a 28,000 in-lb. vibratory moment at $\phi = 142^\circ$. The load arm phasing is shown in Figure A10. This loading resulted in an OOP stiffness of 5×10^6 in-lb/rad. and an IP stiffness of 6×10^6 in-lb/rad.

COMPONENT	OOP (IN-LB/RAD)	IP (IN-LB/RAD)
RING	172×10^6	191×10^6
BRIDGE	-	46×10^6
ARM	118×10^6	2×10^{11}
TOTAL	70×10^6	37×10^6

FIGURE A4. BARREL MOMENT STIFFNESSES



COMPONENT	OOP (IN-LB/RAD)		IP (IN-LB/RAD)	
	A	B	A	B
RING	172×10^6	95×10^6	191×10^6	97×10^6
BRIDGE	—	—	46×10^6	60×10^6
ARM	118×10^6	267×10^6	2×10^{11}	4×10^{10}
TOTAL	70×10^6		37×10^6	

FIGURE A5. EFFECT OF POINT SELECTION FOR BARREL COMPONENT STIFFNESS DETERMINATION

FEA

COMPONENT	OOP (IN-LB/RAD)	IP (IN-LB/RAD)
RING	172×10^6	191×10^6
BRIDGE	—	46×10^6
ARM	118×10^6	2×10^{11}
TOTAL	70×10^6	37×10^6

DESIGN

COMPONENT	OOP (IN-LB/RAD)	IP (IN-LB/RAD)
RING	67×10^6	71×10^6
BRIDGE	—	370×10^6
ARM	675×10^6	675×10^6
TOTAL	61×10^6	55×10^6

FIGURE A6. COMPARISON OF FEA AND DESIGN BARREL STIFFNESS RESULTS

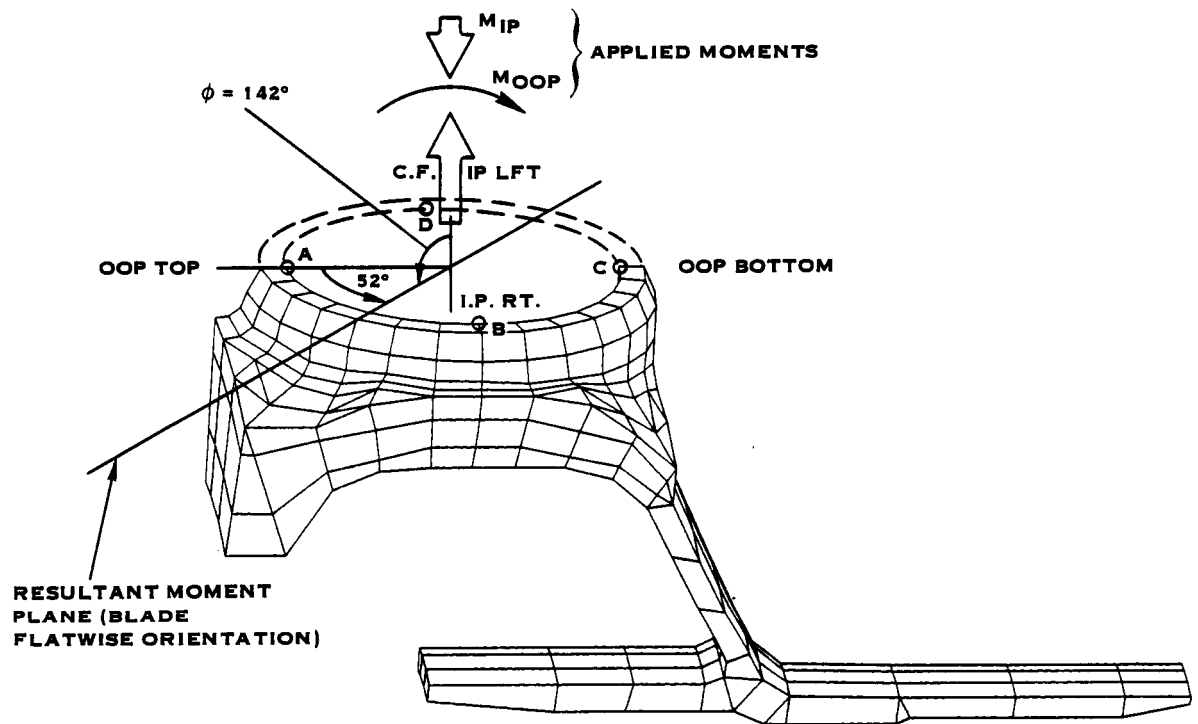
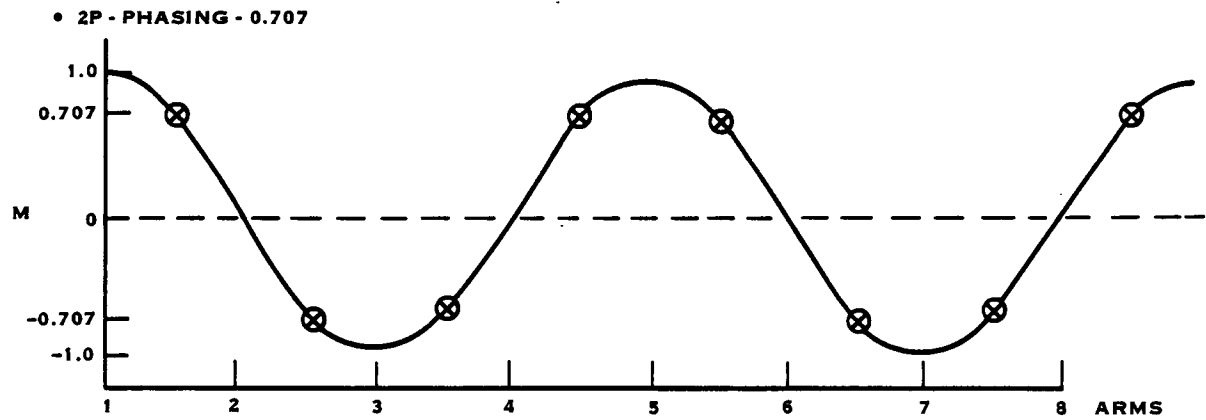


FIGURE A7. 2P APPLIED LOADS



APPLIED LOADS	OOP (IN-LB/RAD)	IP (IN-LB/RAD)
C.F. \pm M		
86,000 + 10,000	16.87×10^6	7.94×10^6
86,000 + 20,000	16.93×10^6	7.80×10^6
86,000 + 28,000	16.92×10^6	7.69×10^6

FIGURE A8. IN-AND OUT-OF-PLANE BENDING
RETENTION STIFFNESS SUMMARY FOR 2P MODE

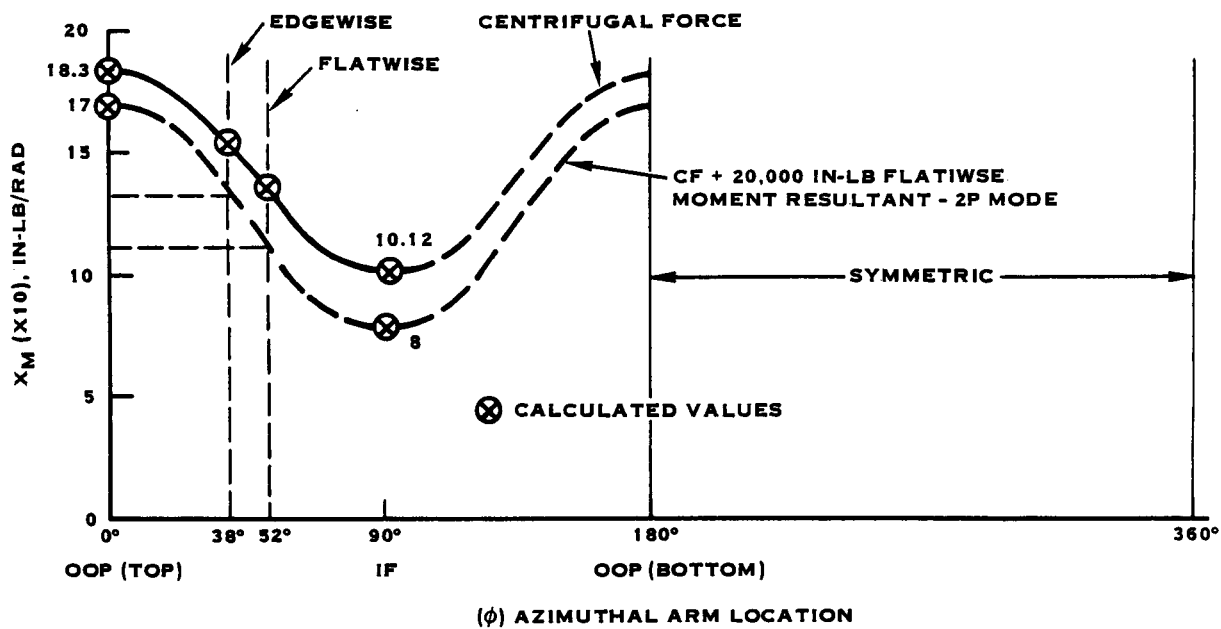
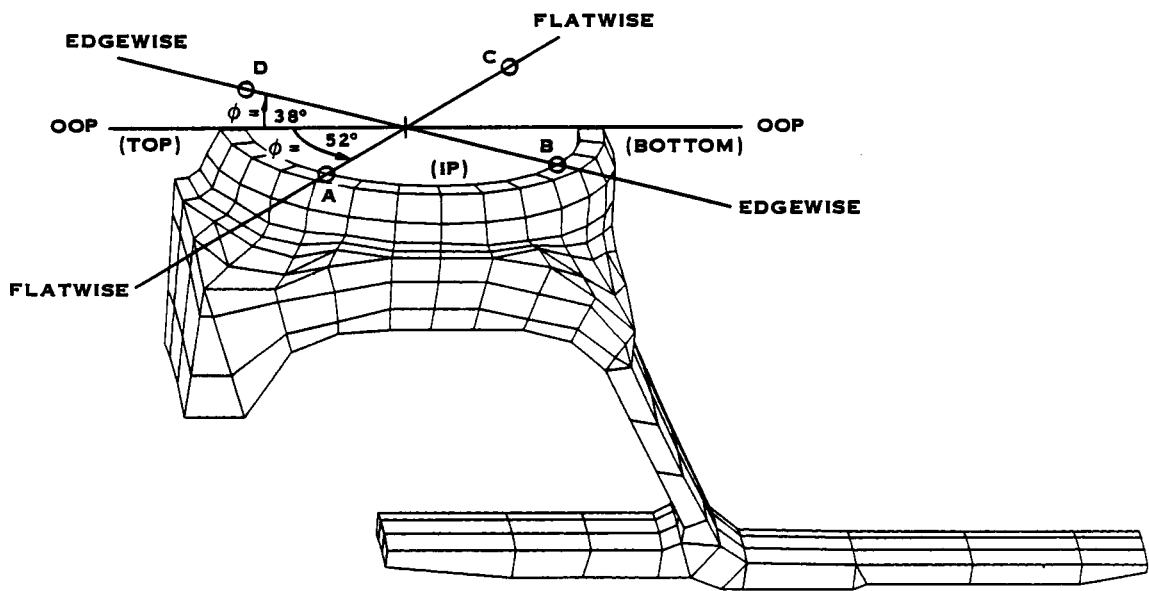


FIGURE A9. 2P FLATWISE AND EDGEWISE RETENTION STIFFNESS DETERMINATION

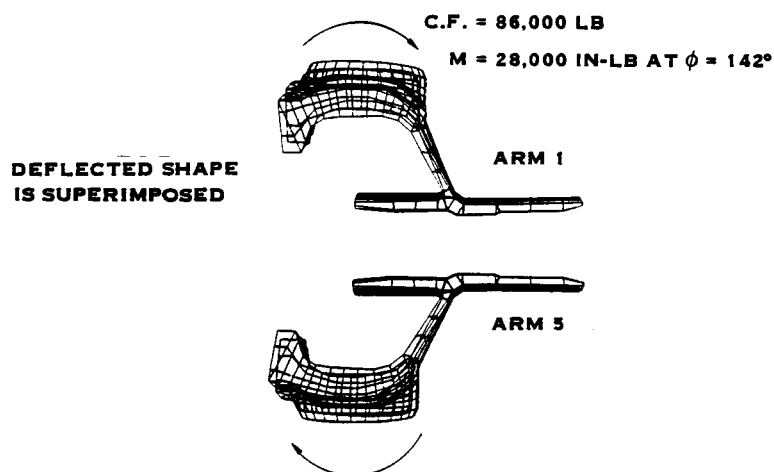
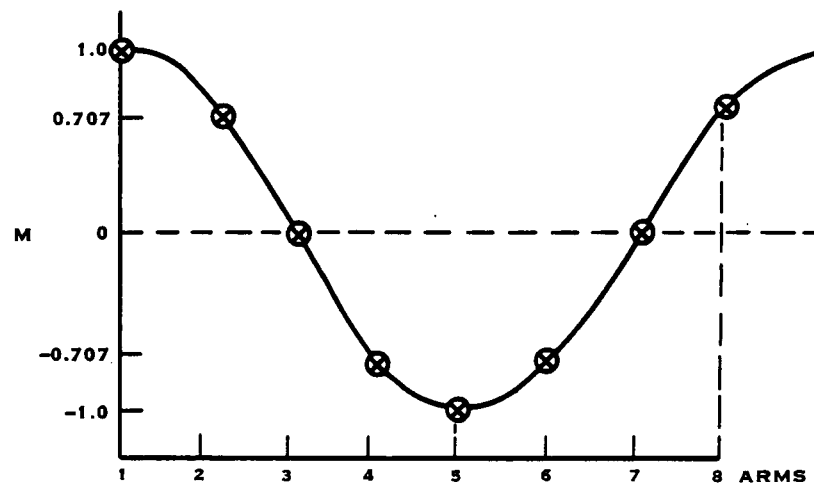
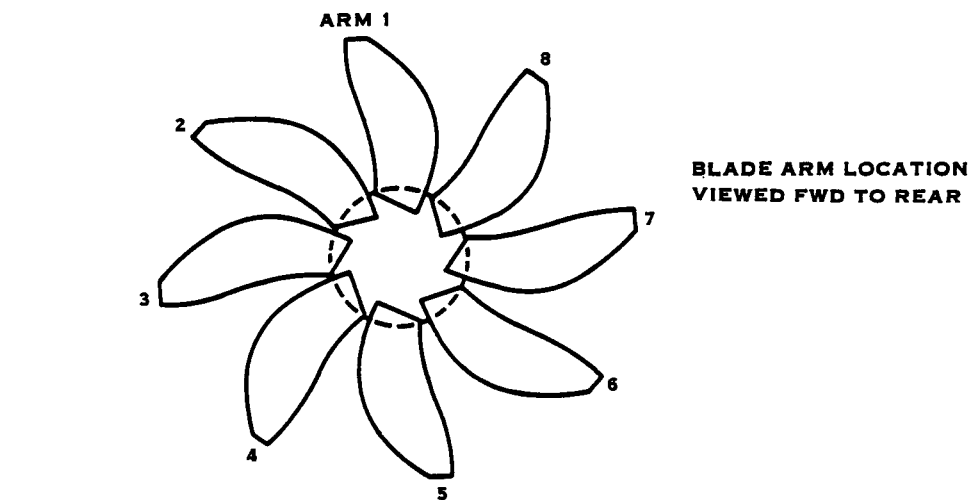


FIGURE A10. 1P LOAD PHASING

Stress Results

Average nodal point equivalent (Von Mises) stresses were evaluated for the centrifugal force, 2P and 1P load cases. Stresses in these cases are predominantly due to the centrifugal force. Stress contours for this case are shown in Figure A11. Peak stress contours are highlighted.

Cyclic stresses resulting from the 1P load case are shown in Figures A12 and A13. Both the right and left segments of arms 1 and 5 are shown because of the asymmetric applied loading. Due to the nonsymmetric response of the barrel, the cyclic stress does not fully reverse. In all the cases surveyed, the stress levels are below the allowables for steel.

Analysis Checks

Several checks were made on the analysis procedure to determine solution sensitivity. The centrifugal force load case was used for these checks because it required the least amount of solution and evaluation time. The first check made was with respect to the selection of the load point on the race. This was done to determine the sensitivity between the load point and the resultant stiffness. Figure A14 shows the two load point locations selected. The first choice is the location used throughout the study. It was felt that this race location was a fair representation of where the ball bearing would be located during the various loadings. The second choice was assumed to be an extreme case that could not occur under normal operating conditions. The load points selected resulted in stiffness differences of less than 2% indicating a low sensitivity to the load point selection.

A solution convergence check was made by constructing a model using 20-noded bricks instead of 8-noded bricks. This increased the number of degrees of freedom from 1,300 to 4,600 without changing the number or distribution of the bricks. A comparison of displacements between the 8-noded and 20-noded model for a centrifugal loading is shown in Figure A15. The 20-noded model results in higher displacements. This translates into an out-of-plane stiffness which is approximately 2% lower than the 8-noded model and 6% lower in-plane. Comparison of stresses shows, as expected, a greater difference; see Figure A16. However, due to the placement of the midside nodes in the 20-noded brick, errors exist in the stresses. Since the stress levels are generally low with regard to the allowables, the stress results do not present a problem.

Summary

The use of 3D finite element analysis coupled with the program F264CL has provided a significant amount of insight into the structural action of the barrel. Both the stiffness and stress levels are within the allowables.

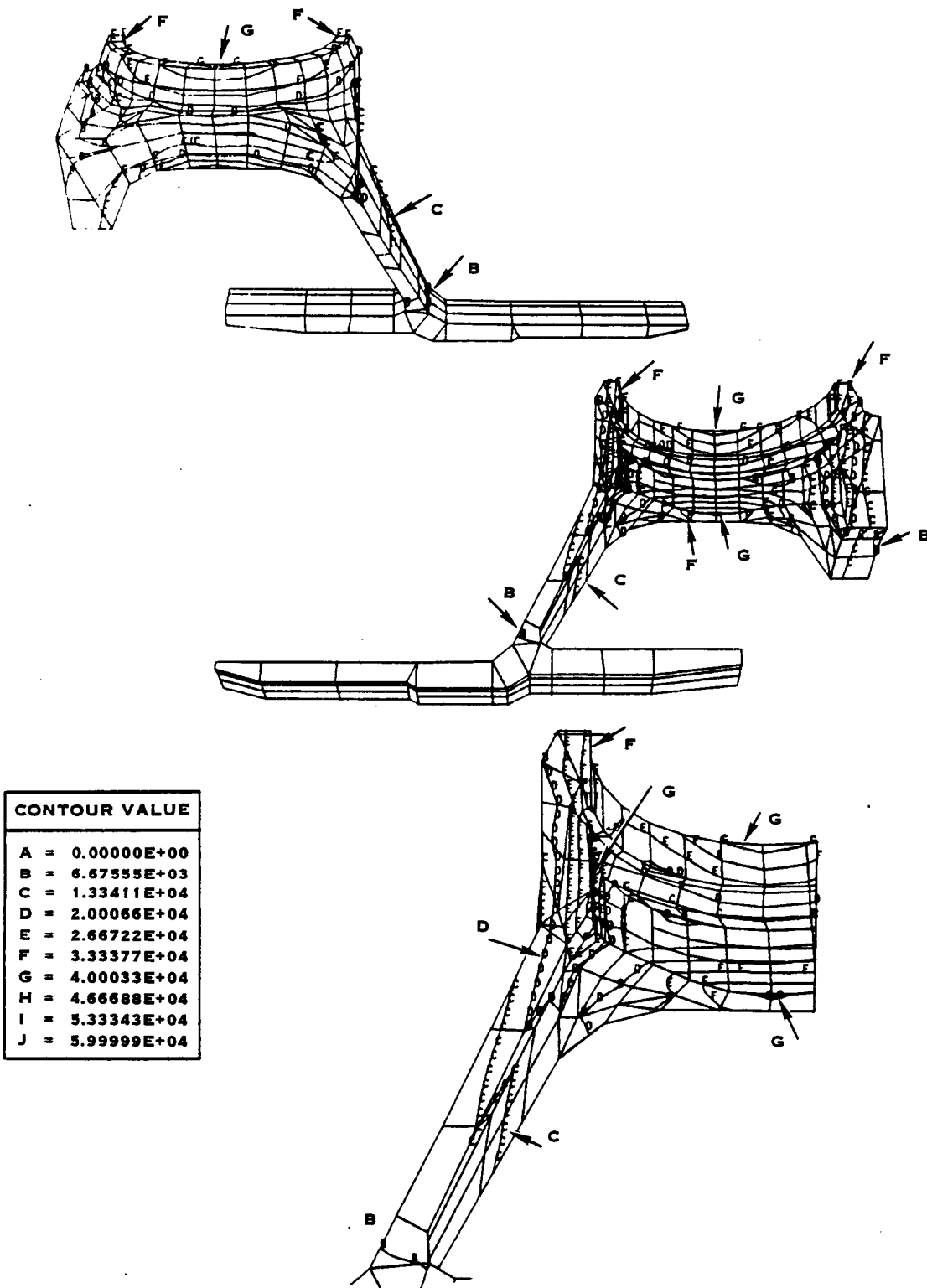


FIGURE A11. CENTRIFUGAL FORCE EQUIVALENT STRESS

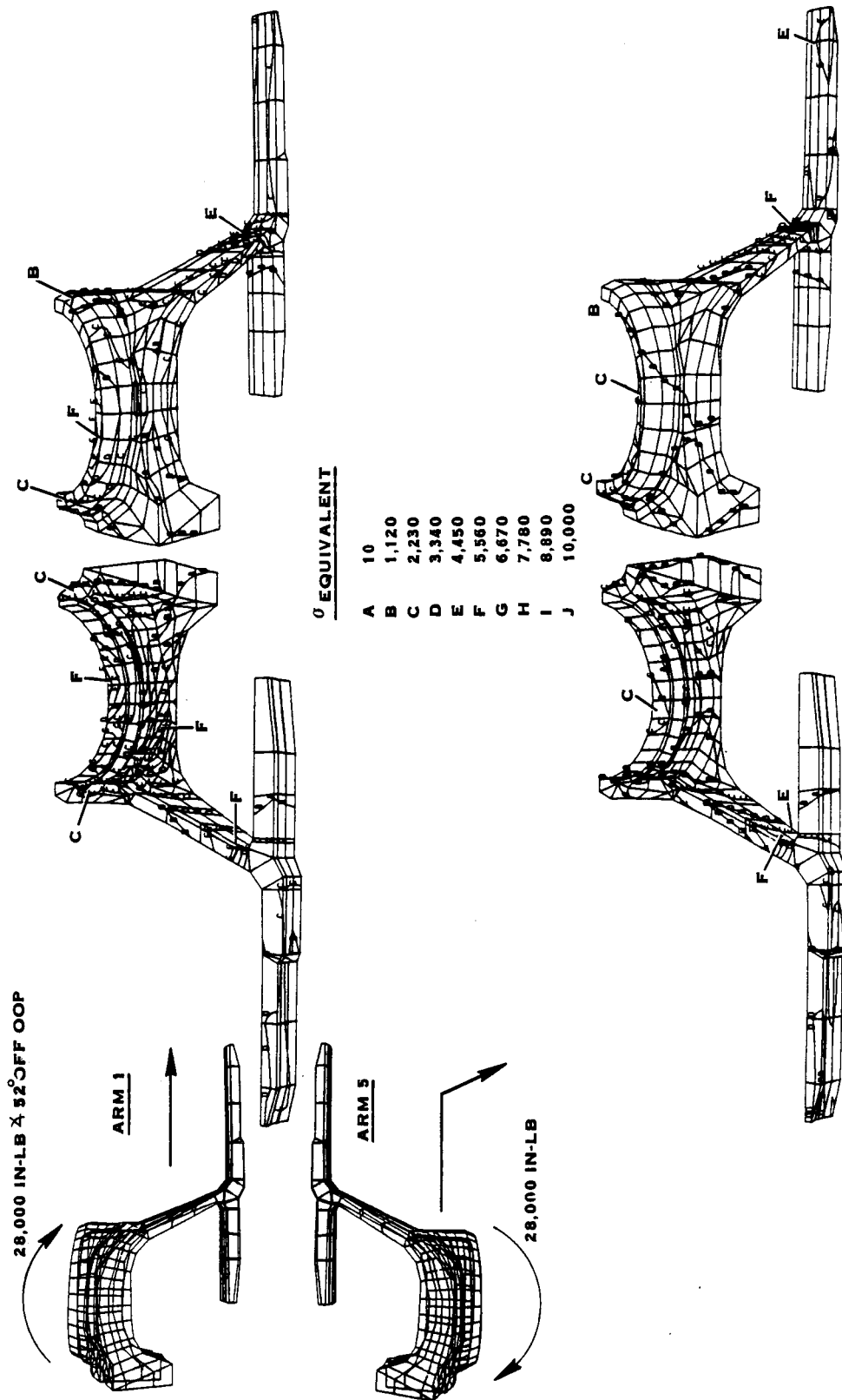


FIGURE A12. 1P - CYCLIC STRESSES ON FULL MOMENT ARM
RIGHT SEGMENT (MAX LOAD)

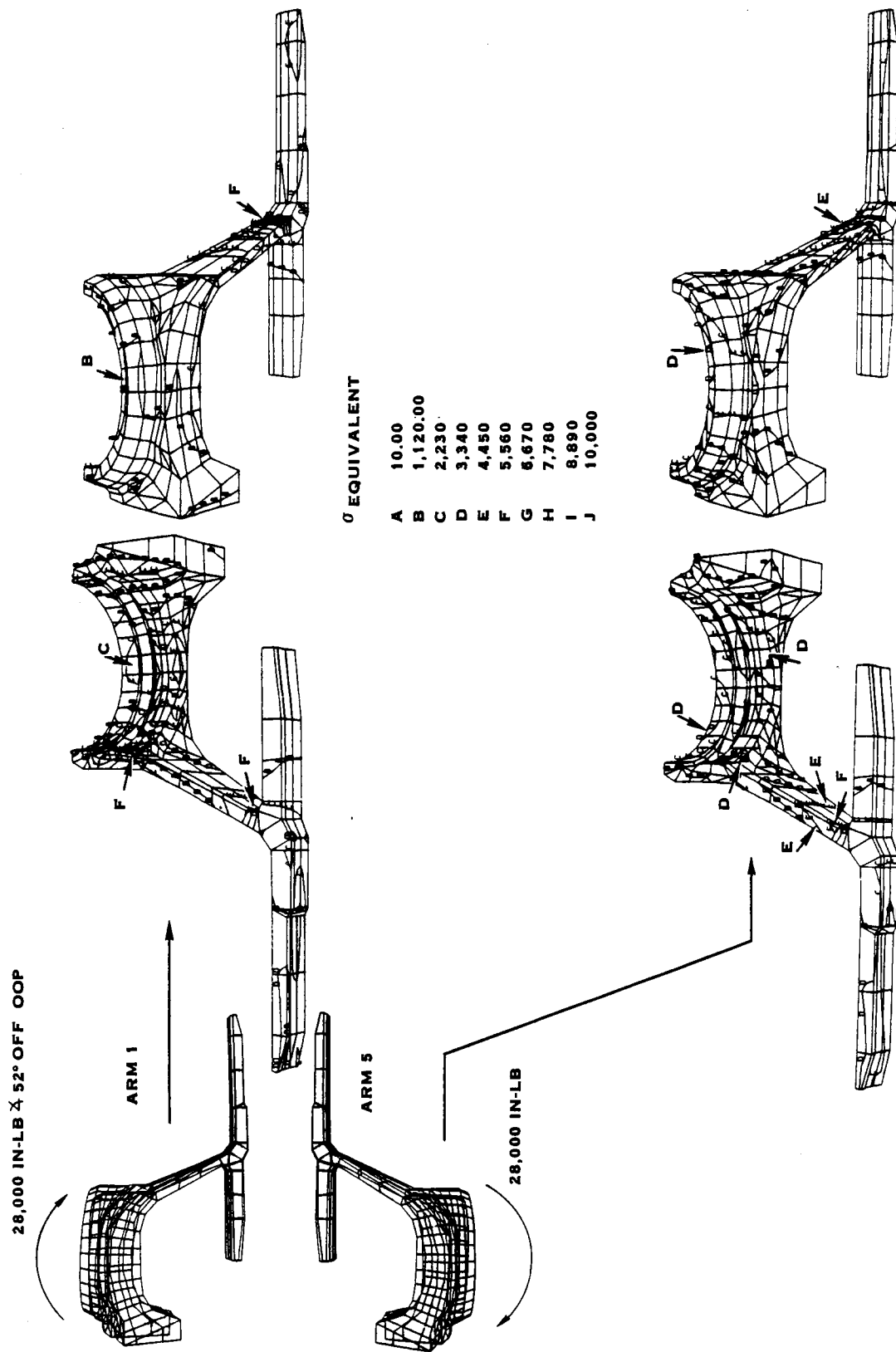
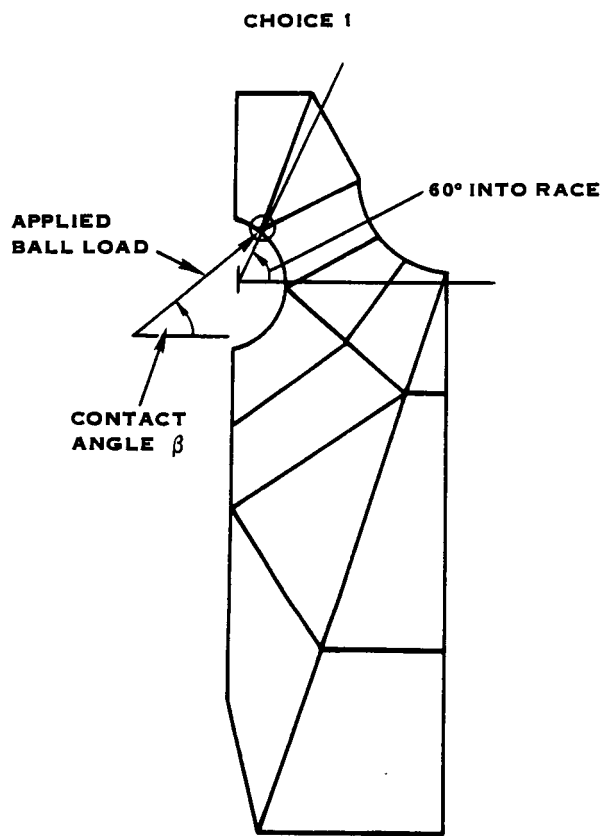
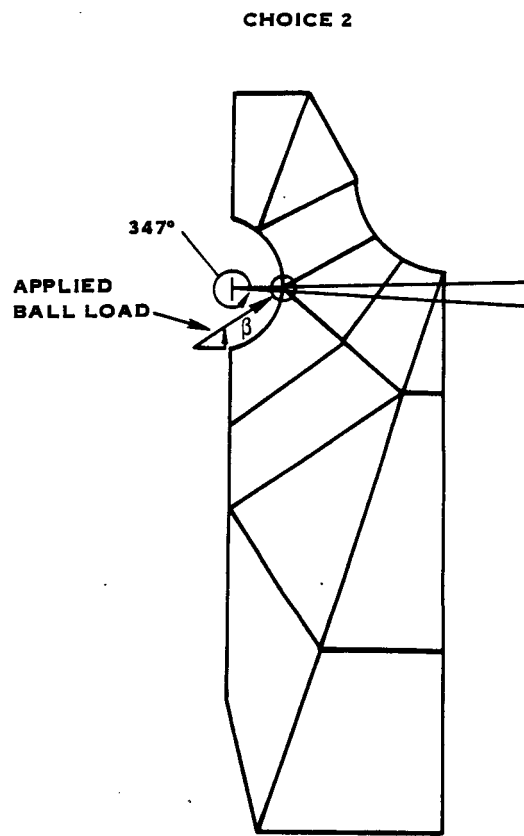


FIGURE A13. IP - CYCLIC STRESSES ON FULL MOMENT ARM
LEFT SEGMENT (MIN LOAD)



K _{IP}	K _{OP}
11.46×10^6	16.84×10^6

$\Delta \%$
 KIP - 2%
 KOOP - 0.5%



K _{IP}	K _{OP}
11.70×10^6	16.92×10^6

FIGURE A14. STIFFNESS SENSITIVITY TO APPLIED LOAD POINT

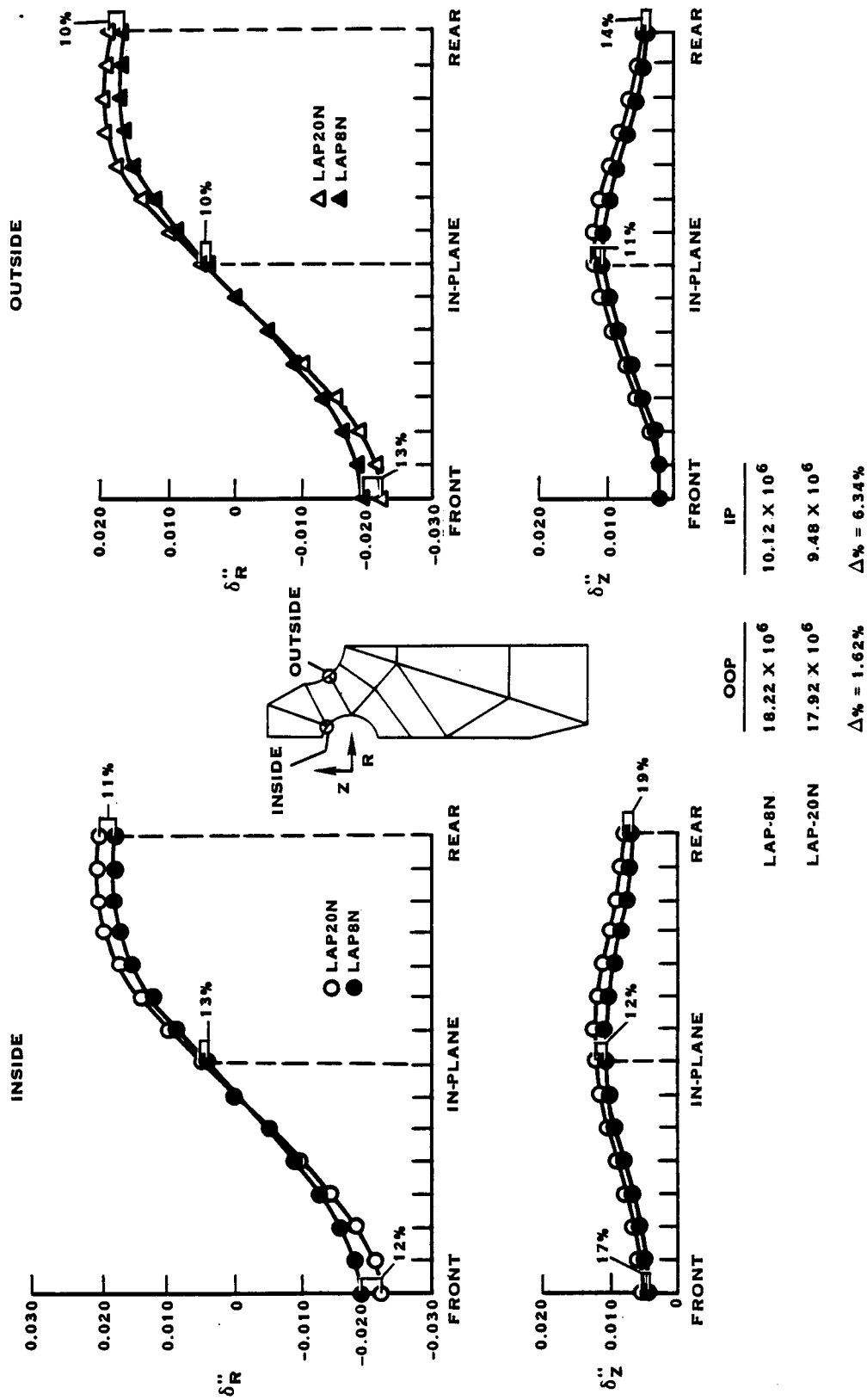
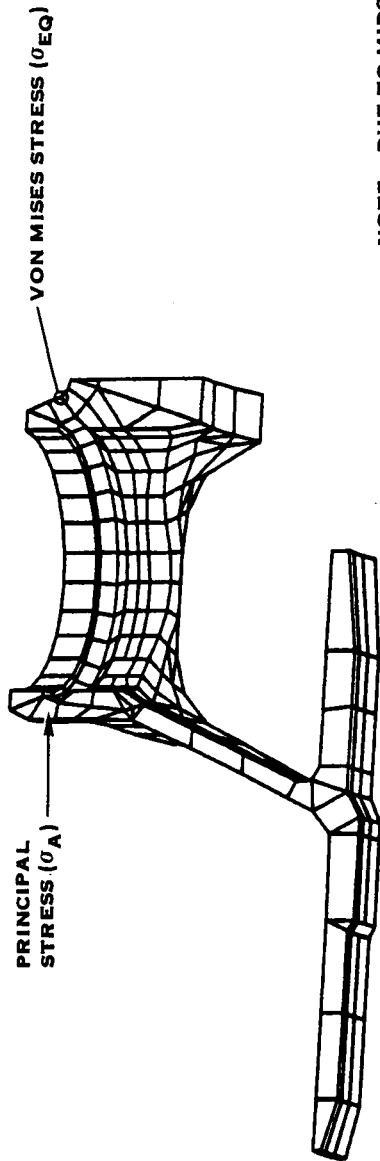


FIGURE A15. COMPARISON OF 8-NODED VERSUS 20-NODED MODELS



NOTE: DUE TO MIDSIDE NODE PLACEMENT ON THE 20N ELEMENT THE STRESSES REPORTED FOR THESE ELEMENTS WILL BE IN ERROR.

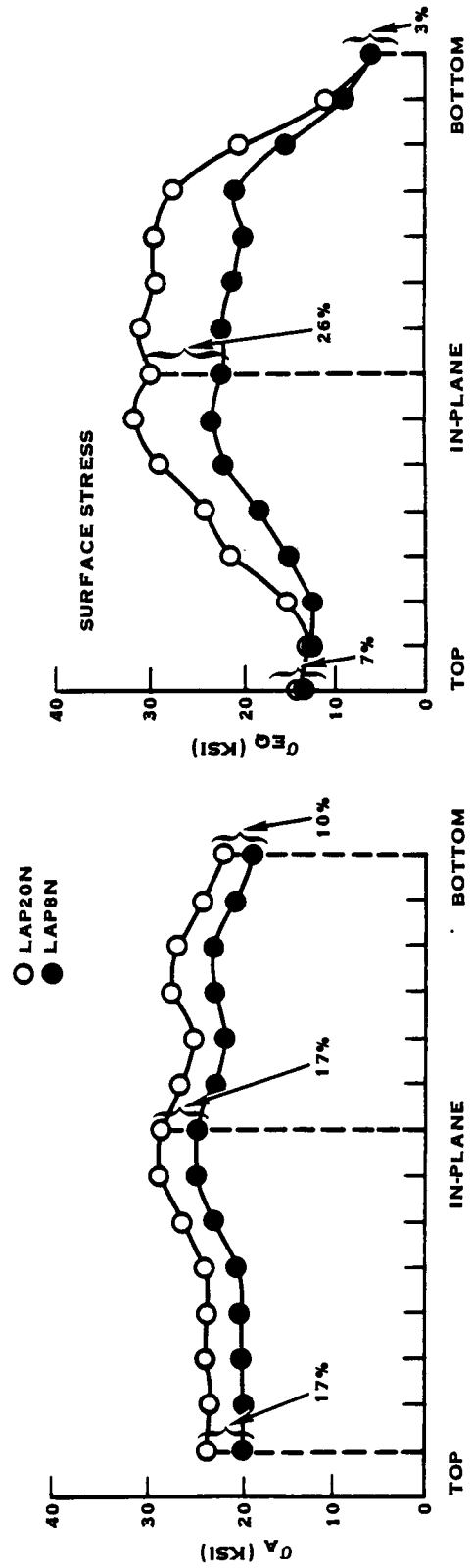



FIGURE A16. COMPARISON OF 8-NODED VERSUS 20-NODED MODELS

APPENDIX B
HUB ASSEMBLY LAYOUT DRAWING L-14325-5

1. Report No. CR 174786		2. Government Accession No.		3. Recipient's Catalog No.	
4. Title and Subtitle Large-Scale Advanced Prop-Fan (LAP) Hub/Blade Retention Design Report				5. Report Date	
				6. Performing Organization Code 535-03-12	
7. Author(s) Matthew Soule				8. Performing Organization Report No. HSER-9247	
9. Performing Organization Name and Address Hamilton Standard Division United Technologies Corporation P.O. Box 1000 Windsor Locks, Connecticut 06096				10. Work Unit No.	
				11. Contract or Grant No. NAS 3-2351	
12. Sponsoring Agency Name and Address National Aeronautics and Space Administration Washington, D.C. 20546				13. Type of Report and Period Covered Contractor Report	
				14. Sponsoring Agency Code	
15. Supplementary Notes Project Manager, David A. Sagerser, Advanced Turbo Prop Project Office, NASA Lewis Research Center, Cleveland, Ohio 44135					
16. Abstract In recent years, considerable attention has been directed toward improving aircraft fuel consumption. Studies have shown that blades with thin airfoils and aerodynamic sweep can extend the inherent efficiency advantage of turboprop propulsion systems and may now be extended to the higher speed of today's aircraft. Hamilton Standard has designed a 9-foot diameter single-rotation Prop-Fan and is now in the process of manufacturing this system. The hardware will be tested on a static test stand, a low speed wind tunnel and a research aircraft. The major objective of this testing is to establish the structural integrity of large-scale Prop-Fans of advanced construction in addition to the evaluation of aerodynamic performance and the aero-acoustic design. This report covers the design analysis of the Large-Scale Advanced Prop-Fan Hub/blade retention assembly. Specifically, analysis of the retention area of the blade shank, blade retention, hub, and tailshaft are covered. Subjects included are stress and strain analysis, material hardness requirements, weight predictions and stiffness characteristics.					
17. Key Words (Suggested by Author(s)) Prop-Fan Hub Structural Design			18. Distribution Statement 		
19. Security Classif. (of this report) Unclassified		20. Security Classif. (of this page) Unclassified		21. No. of Pages 74	
22. Price*					